ARMY RESEARCH LABORATORY

The High Strain Rate Deformation of Tungsten Single Crystals

Edward J. Horwath

ARL-TR-620 November 1994

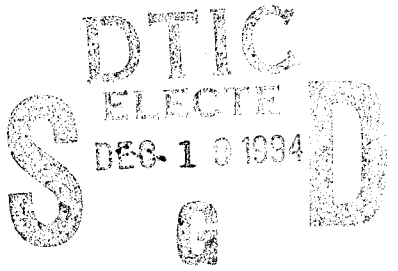

NOTICES

Destroy this report when it is no longer needed. DO NOT return it to the originator.

Additional copies of this report may be obtained from the National Technical Information Service, U.S. Department of Commerce, 5285 Port Royal Road, Springfield, VA 22161.

The findings of this report are not to be construed as an official Department of the Army position, unless so designated by other authorized documents.

The use of trade names or manufacturers' names in this report does not constitute indorsement of any commercial product.

REPORT DOCUMENTATION PAGE

Form Approved
OMB No. 0704-0188

1. AGENCY USE ONLY *(Leave blank)*	2. REPORT DATE	3. REPORT TYPE AND DATES COVERED
	November 1994	Final, Aug 92–Apr 94

4. TITLE AND SUBTITLE

The High Strain Rate Deformation of Tungsten Single Crystals

5. FUNDING NUMBERS

PR: 1L162618AH80

6. AUTHOR(S)

Edward J. Horwath

7. PERFORMING ORGANIZATION NAME(S) AND ADDRESS(ES)

U.S. Army Research Laboratory
ATTN: AMSRL-WT-TA
Aberdeen Proving Ground, MD 21005-5066

8. PERFORMING ORGANIZATION REPORT NUMBER

9. SPONSORING / MONITORING AGENCY NAME(S) AND ADDRESS(ES)

U.S. Army Research Laboratory
ATTN: AMSRL-OP-AP-L
Aberdeen Proving Ground, MD 21005-5066

10. SPONSORING / MONITORING AGENCY REPORT NUMBER

ARL-TR-620

11. SUPPLEMENTARY NOTES

12a. DISTRIBUTION / AVAILABILITY STATEMENT

Approved for public release; distribution is unlimited.

12b. DISTRIBUTION CODE

13. ABSTRACT *(Maximum 200 words)*

Samples of single-crystal tungsten, in three orientations ([100], [110], [111]), were compressively deformed at high strain rates (1,000–2,000 s^{-1}) using a Kolsky (split-Hopkinson) type pressure bar apparatus. Samples of the single-crystal tungsten were also deformed at low strain rate (0.0001 s^{-1}) using a conventional load frame. The [110] orientation exhibited constraint of flow consistent with twofold crystal symmetry about this axis, resulting in skewed flow and noncylindrical specimens after the Kolsky bar test. Both the [111] and [110] orientations exhibited a yield or load drop phenomenon. This load drop may have been associated with either: 1) lack of screw dislocation cross slip at high strain rate; 2) twinning of the crystal lattice; or 3) interstitial solute atoms such as nitrogen or carbon pinning dislocations. As a result of this load drop for the lower symmetry [111] and [110] orientations, the quasi-static (0.0001 s^{-1}) test had higher flow stress for a given strain than the higher strain rate tests with the Kolsky bar. The [100] orientation crystals exhibited uniform deformation and high rate of work-hardening at both low and high strain rates. The unique behavior of these crystals is postulated in terms of the crystal symmetry, structural evolution at various strain rates, and dislocation flow mechanisms.

14. SUBJECT TERMS

tungsten, deformation, high strain rate, single crystals

15. NUMBER OF PAGES

58

16. PRICE CODE

17. SECURITY CLASSIFICATION OF REPORT	18. SECURITY CLASSIFICATION OF THIS PAGE	19. SECURITY CLASSIFICATION OF ABSTRACT	20. LIMITATION OF ABSTRACT
UNCLASSIFIED	UNCLASSIFIED	UNCLASSIFIED	UL

INTENTIONALLY LEFT BLANK.

ACKNOWLEDGMENTS

The author would like to thank Dr. William Bruchey for his considerable interest and initial conception of the unique project using single-crystal tungsten samples.

The author would also like to thank Dr. Ramesh at Johns-Hopkins University for making his equipment available for the Kolsky bar test and for his guidance and support during the project.

Finally, the author would like to express his appreciation to Mr. Gordon Dudder, Battelle Pacific Northwest Laboratory, for sample preparation and for generating the slow strain rate compression data referenced in this report.

INTENTIONALLY LEFT BLANK.

TABLE OF CONTENTS

INTENTIONALLY LEFT BLANK.

LIST OF FIGURES

1. INTRODUCTION

Tungsten is of interest in ballistic applications due to its high density, considerable strength during mechanical loading, and limited environmental concerns compared to depleted uranium. In addition, tungsten heavy alloys (85%–97% tungsten) used in armor-piercing kinetic energy (KE) penetrators have a two-phase microstructure consisting of *single-crystal tungsten particles* in a matrix of W-Ni-Fe or other alloy. The high content of tungsten in these penetrator materials, in single crystal or oriented crystalline form, provides good strength and density and also influences the mechanical and deformation behavior of these composites. The deformation mechanisms which occur in these tungsten particles during the ballistic penetration of W-Ni-Fe composite penetrators into armor steels could subsequently influence the penetration capability of the KE round.

Previous papers by Bruchey et al. (1993) have investigated the ballistic performance of tungsten in single crystal form and found significant contributions to the ballistic performance occurred due to crystallographic orientation and dislocation/slip mechanisms. The [100] orientation penetrator rods had superior ballistic performance to [111] or [110] single-crystal rods. The differences in performance were associated with a combination of crystal flow strength, and ability to flow material through crystal dislocation movement in the back eversion process during a ballistic penetration event (see papers by Bruchey et al. 1993 and Herring 1992). The exact material flow mechanisms responsible for material eversion during the single-crystal penetration process are not fully understood, but Herring (1992) (research done in conjunction with these authors) has shown that movement of screw dislocations is primarily responsible for this deformation. In addition, Herring has pointed out that crystal symmetry and angle of slip planes with the stress axis contributes to the flow mechanisms and ballistic performance. However, the exact nature of flow mechanisms at high strain rate for a particular tungsten single-crystal orientation remains unclear.

Consequently, an investigation was initiated to determine the high strain rate mechanical behavior of single-crystal tungsten samples. This paper presents additional work completed concerning the high strain rate deformation of single-crystal samples of tungsten using the Kolsky (Split-Hopkinson) type apparatus.

2. SAMPLE DESCRIPTION

Single-crystal tungsten samples were grown by Atomergic Chemetals in three orientations ([100], [110], [111]) from 99.99 pure starting stock by Czochralski technique and or strain anneal process (same material as used in previous ballistic tests) (see papers by Bruchey 1993). Kolsky bar samples were sectioned with an abrasive diamond saw, at slow cutting speed so as to minimize damage and depth of the disturbed surface layer. These samples (6.9 mm dia. x 6.9 mm length) of single-crystal tungsten were then compressively deformed at strain rates of 1,000–2,000 s^{-1}, using a Kolsky (split-Hopkinson) pressure bar apparatus (Kolsky 1949; Coates and Ramesh 1990; Follansbee and Frantz 1983). The specimen size and compression bar diameter were carefully selected to eliminate the detrimental effects of radial inertia, as described by Bertholf and Karnes (1975). The following criteria after Bertholf and Karnes need to be simultaneously satisfied if radial inertia effects are to be minimized:

$$D\,\dot{\bar{\varepsilon}}_s < 5{,}000 \text{ cm s}^{-1}$$

and

$$t / D > 16\mu\text{s cm}^{-1}$$

where D is the diameter of the Kolsky bar, t is the rise time of the incident pulse, and $\dot{\bar{\varepsilon}}_s$ is the mean strain rate.

With rise times of 30–50 μs, a bar diameter of 1.25 cm, and mean strain rates of from 1,000–2,000 s^{-1}, both criteria above are satisfied.

3. KOLSKY COMPRESSION BAR

A standard Kolsky compression bar configuration was used during these experiments. This geometry is well-known and is described in detail in several of the listed references (Kolsky 1949; Lindholm 1964; Davies and Hunter 1963; Follansbee and Frantz 1983). This test series incorporated 12.5-mm-diameter Teledyne VascoMax C350 Maraging steel projectile, input, and output bars. The gas gun to launch striker bars had a 25-mm bore and a travel of 0.88 m. A projectile bar of length 200 mm was used at appropriate velocities of 20–60 m/s to generate appropriate pulses for strain rates of 1,000–2,000 s^{-1}. The incident

and transmitted bars (input and output) were approximately 1 m long, with Micro-Measurements foil resistance strain gauges model MM WK-06-250BF-10C bonded to the bars with Loctite elastomeric modified methacrylate adhesive. The gauges were installed in pairs, with each gauge at nominally the same axial location and 180° apart on the circumference of the bar.

A momentum trap was employed to capture the transmitted pulse, thereby reducing the incidence of failure of strain gauges. This momentum trap consisted of an additional bar of length greater than the projectile bar, located at the end of, and in contact with, the output bar.

A Nicolet model 4094C digital oscilloscope with 4570 plug-ins was used to record incident, transmitted, and reflected wave pulses. Initial tests to determine correct pulse shaping to maintain as constant a strain rate as possible indicated that buffer materials would be required. Consequently, for the [100] and [111] samples, a 0.78-mm Cu buffer was used to shape the incident bar pulse, while a 0.97-mm Al buffer was used to shape the pulses for the [110] crystals.

4. DATA ANALYSIS

Analysis of transmitted and reflected pressure waves (oscilloscope traces) allowed determination of stress and strain in the compression tested samples. From the transmitted pulse, the specimen stress state is determined from:

$$\bar{\sigma}_s = \frac{EA_b}{A_s}\varepsilon_T$$

while from the reflected pulse, the specimen strain is:

$$\bar{\varepsilon}_s = \frac{2c_o}{l_o}\int_0^{\tau}\varepsilon_R dt$$

where E is the bar modulus, l_o is the specimen length, A_b is the bar cross-sectional area, A_s is the specimen cross-sectional area, ε_t is the transmitted strain pulse, c_o is the bar wave velocity, ε_R is the reflected strain pulse, and t is time. The strain rate is integrated over time to obtain the specimen strain history, and correlation with stress history gives an accurate picture of the sample stress vs. strain response at the strain rate found above.

In the analysis described previously, the oscilloscope data is first edited with the software program Vu-point to clip portions of interest. A dispersion correction program similar to that of Follansbee and Frantz was then applied to the oscilloscope signals. The strain rate pulse was then integrated to obtain specimen strain history. Both stress and strain data were then converted to axial true stress, and axial true strain using the strain history data and assuming a homogeneous state of deformation. See Coates and Ramesh (1990) for additional data analysis methodology.

5. RESULTS

5.1 True Stress vs. True Strain Curves. The initial analysis of oscilloscope tracings generated data concerning the true stress, true strain, and strain rate in the samples. Figures 1–24 present data for each of the crystal orientations investigated, where two samples of each orientation, at somewhat different strain rates, were loaded with the Kolsky apparatus. Figures 1, 5, 9, 13, 17, and 21 present *true strain vs. time* data for each of the tests. Figures 2, 6, 10, 14, 18, and 22 present *true stress vs. time* data for each of the tests. Figures 3, 7, 11, 15, 19, and 23 present *true stress vs. true strain* data for each of the tests. And, Figures 4, 8, 12, 16, 20, and 24 present *strain rate vs. time* data for each of the tests.

Table 1 presents a summary of the test data presented in Figures 1–24 and parameters associated with each single-crystal orientation.

Table 1. Summary of Test Data Presented in Figures 1–24

Crystal	Test No.	Figures	Nominal Strain Rate	Maximum Stress (GPa)	Total Strain
[100]	1	1, 2, 3, 4	1625	1.81	0.15
[100]	2	5, 6, 7, 8	1250	1.75	0.11
[111]	1	9, 10, 11, 12	1225	1.86	0.11
[111]	2	13, 14, 15, 16	1425	1.80	0.12
[110]	1	17, 18, 19, 20	1950	1.06	0.17
[110]	2	21, 22, 23, 24	1350	1.11	0.11

The strain rates indicated in this table are the average values associated with each test. The stress-strain data is presented for axial compressional loading and does not reflect shear stress or strain on a particular slip system. Analysis of the stress-strain data with respect to a particular slip system will be presented in a later section of this paper.

In analyzing the data summarized in Table 1 and in Figures 1–24, it is important to consider factors which might indicate less than optimal test conditions. These factors include nonlinearity of the strain with time, variation of strain rate with time, and abrupt and unexplained changes in true stress with time. In general the results were satisfactory, although Test 2 [110] orientation had a somewhat nonlinear strain-time history and an abrupt load change at 70 μs after load initiation.

The following sections discuss specific observations associated with the Kolsky bar results presented in Figures 1–24.

5.2 Yield Phenomena. Yielding followed by load drop takes place for the [111] and [110] crystal orientations (see Figures 11, 15, 19, and 23). However, it should be noted that no data are presented for yield stress or elastic modulus in Table 1. The analysis of Kolsky bar data ignores some early part of the sample loading during ≈5 reflections of the plastic wave within the sample, corresponding to the time required for the attainment of uniform stress in the specimen. This would be on the order of 15 μs for this specimen geometry. It should also be remembered that dispersion contributes oscillations to the shape of the stress-strain curves. However, for single-crystal deformation, the localized nature of deformation on slip systems, as well as the variation in wave speed with crystal lattice direction, may make this early portion of the loading curve more important and informative than respective portions of polycrystalline sample load histories.

Therefore, there is justification in stating that the early portions of these curves are truly indicative of the actual single crystal response to compression loading, in that the curves do show more pronounced yield phenomena for the lower symmetry systems [110] and [111]. As other researchers, Garlick and Probst (1964), Argon and Maloof (1966), Rose, Ferriss, and Wulff (1962), and Beardmore and Hull (1965), have observed in both tension and compression tests, orientations close to [110] or [111] did indeed display yielding phenomena. This yielding might be associated with: 1) Stage two type easy glide on one slip system, possibly (110) [111], without much cross-slip or activation of other slip systems immediately; 2) Twinning of the structure at high strain rate as observed for BCC iron by various

researchers (Leslie 1973); 3) Dislocation pinning by interstitial solute atoms such as carbon or nitrogen (after Cottrell 1953). Especially for the twofold symmetry [110] crystals, there appears to be a large load drop associated with this glide or twinning period, followed by slow work-hardening, as dislocations find difficulty in freely gliding after some interacting and tangling in the orientation. The high symmetry orientation [100] crystals (see Figures 3 and 7) exhibited no yielded phenomena and a considerable rate of work-hardening, as observed by other researchers in slow strain rate tension tests (Garlick and Probst 1964; Argon and Maloof 1966; Rose, Ferriss, and Wulff 1962).

5.3 Flow Stresses and Work-Hardening Rate. Often the compressive flow stresses (evaluated at a fixed strain in the sample) are compared at various strain rates. This allows some understanding of the strain rate sensitivity of the flow stress of the particular material of interest. Figure 25 presents a summary of the flow stress strain rate dependence, while Figures 26, 27, and 28 present true stress vs. true strain data for each crystal orientation at various strain rates. However, we do not have sufficient data to make an estimate of the flow stress rate dependence for each orientation. (Note the variation in the shapes of the stress-strain curves at high strain rates in Figures 27 and 28.) In general, it appears that the [100] and [111] orientation appear to exhibit similar flow stresses at the higher strain rates. The [100] orientation has much lower flow stress at all strain rates.

In regards to the work-hardening rate, it is fairly clear that the [110] work-hardening is minimal, Figure 28, as expected for this low symmetry orientation. The [100] orientation does appear to work harden extensively compared to both orientations.

5.4 Shear Stress vs. Shear Strain. The actual shear stresses and strains on appropriate slip systems may be calculated after Bowen and Christian (1965). The appropriate equations used to determine shear stresses and shear strains are:

shear strain:

$$\gamma = \frac{\left[\left(\frac{\ell_o}{\ell}\right)^2 - \sin^2 \theta_o\right]^{\frac{1}{2}} - \cos \theta_o}{\cos \lambda_o}$$

shear stress:

$$\tau = \frac{L}{A_o}\left(\frac{\ell}{\ell_o}\right) \cos\lambda_o \left[1 - \left(\frac{\ell}{\ell_o}\right)^2 \sin^2 \theta_o\right]^{\frac{1}{2}},$$

where:

λ_o = initial angle between stress axis and slip direction

θ_o = initial angle between stress axis and normal to slip plane

ℓ_o = initial sample length

ℓ = sample length at any point during test

A_o = initial cross-sectional area of sample

L = axial compression load on sample.

If initial dislocation motion is assumed to occur on (110) [111] slip systems, then appropriate analysis of the initial axial true stress vs. true strain data previously presented yields the shear curves in Figures 29–31. The curves were generated by using a basic program to convert data through the above equations of Bowen and Christian.

The actual shear stresses on the (110) planes for the various crystal orientations are substantially lower than the axial compression stresses. Although the Kolsky bar apparatus does not generate accurate data in the initial 15 μs or 20 μs, it is apparent that the stresses to initiate plastic deformation on these planes are small. The load drop phenomena (easy glide or twinning as discussed previously) in the [110] and [111] crystals occurred at 0.4 GPa–0.5 GPa (60–70 psi) at these loading rates of between 1,000–2,000 s^{-1} (see Figure 31). After load drop, the shear stresses required for plastic flow in (110) crystals on slip planes were as low as 150 GPa (21 psi). Actual proportional limits (onset of plastic deformation) could not be determined accurately because of the nature of the Kolsky bar experiment.

Also interesting are the higher stresses required on the [100] planes to continue deformation to large strains. These higher stresses and large rate of work-hardening are related to the fourfold symmetry of this crystal, with consequent early initiation of dislocation motion on various (110) planes, and more frequent cross-slip and tangling of dislocations.

Finally, these calculations are made assuming that slip continues to occur on one slip system, which is probably not a valid assumption after several percent strain. At some point, double slip would occur etc., and the calculations would need revision. The curves have been included to present a general picture of the shear stresses and shear strains on the most favorable slip system.

5.5 Slip Traces and Slip Systems. The Kolsky bar samples were examined after test with the scanning electron microscope to investigate slip traces on the sample surface. The [110] and [111] orientations showed pronounced slip traces on the surfaces (Figures 34, 35, 36, 37, and 38) most likely corresponding to (110) [111] type slip. The [100] orientation samples (Figures 32 and 33) had smooth surfaces and no large-scale slip markings.

The [100] orientation samples showed evidence of the crack nucleation method after Cottrell (1953). See Figure 32 (A and B), where fracture is apparent on (100) planes both perpendicular and parallel to the [100] penetrator axis. According to Cottrell (1953) two partials on [111] can combine to form a void on [100] as:

$$\frac{a}{2}[111] + \frac{a}{2}[1\bar{1}1] \rightarrow a[100]$$

The higher strains encountered in the first [100] crystal tested caused sample failure on these cleavage planes, again see Figures 32a and 32b. The second [100] crystal tested showed some incipient cracks forming on these (100) planes, but large-scale failure did not occur because of the smaller sample strain. Both samples had smoother surfaces than [110] or [111] orientation crystals because of the more uniform deformation on numerous slip planes, associated with the fourfold symmetry of this orientation.

The [111] and [110] samples showed evidence of large-scale deformation on a reduced number of slip planes. Especially for the [110] orientation, Figures 36a and 36b, the constraint due to the twofold symmetry was severe, and the samples became ellipsoidal in cross-section after the Kolsky bar test. Large slip traces for the (110) [111] slip system are seen on the sample surface. The [110] samples also showed some evidence of incipient failure on a macro-scale, as plastic deformation on the few available slip planes eventually exhausted the ability of the lattice to smoothly move dislocations.

For the [111] orientation figures, much evidence is again seen for extensive slip on (110) [111] type systems. The final sample geometry here is quite unique, where the samples had larger cross-sections adjacent to the Kolsky bar apparatus, as compared to the sample center. The [111] sample shape may be loosely described as an hourglass after test. This shape is most likely related to the easy movement of screw dislocations in the [111] direction and will be discussed in some detail later. Failures of [111] Kolsky bar samples revealed a different failure mechanism than that exhibited by [100] crystals, with fracture surfaces appearing irregular and nonplaner (see Figure 35).

6. DISCUSSION OF RESULTS

In the previous sections of this paper some interesting aspects of the behavior of single crystals under compressional loading were discussed. In particular, it was found that:

1. Low symmetry orientation crystals, [110] and [111], displayed some type of yield point or load drop when tested at high strain rate.

2. For [110] and [111] crystals, after load drop, the flow stress of the material was substantially reduced and the sample work-hardening rate was low.

3. The work-hardening rate for the [100] crystal was the highest, considerably higher than the [110] crystal orientation work-hardening rate.

4. The [100] orientation crystal flow stress at low (0.0001 s^{-1}) and high (1,000–2,000 s^{-1}) strain rates behaved in a more traditional fashion, with increase in flow stress with strain rate.

5. The [110] orientation crystals after test appeared to be ellipses in cross section, indicative of the twofold symmetry of the crystal.

6. The [100] orientation samples had fairly smooth surfaces after test and microscopic evidence of slip, while the [110] and [111] orientation crystals showed very distinct evidence of large amounts of slip on (110) planes (slip traces on the sample surfaces).

This behavior described previously may be explained in terms of the crystal symmetry, and dislocation motion, with the understanding that the structural evolution at low and high strain rates may be quite different in single crystals.

For the [100] crystal orientation, the Kolsky bar deformation was the most homogeneous and produced the smoothest sample surfaces after test. This is most likely evidence of slip on many slip planes {110} and {112}. The [100] crystal has four symmetrical [111] slip directions 45° apart, with four {110} and two {112} planes which have reasonable Critical Resolved Shear Stress (CRSS) factors of 0.41 and 0.47 respectively. The stress on a pure screw dislocation in this orientation would be [cos(54.7) × axial stress], thereby favoring a high screw component (Herring 1992). The large number of slip systems and the large screw nature of the dislocations would produce a tangled and very dense dislocation network that would result in considerable work-hardening. The large number of slip systems might have eliminated the yield and load drop phenomena as seen in lower symmetry [110] and [111] orientations and most likely produced the high rate of work-hardening observed for this orientation crystal. In this orientation crystal, the structure evolution at low and high strain rates may be similar, in that cross-slip and dislocation tangling continues to occur even at high strain rate due to the large number of operable slip systems.

For the [110] crystal orientation, examination of the specimen geometry after test (see Figures 36a and 36b) indicates that the deformation in the sample was severely constrained due to the few slip systems available. The sample surfaces showed evidence of {110} and/or {112} slip systems deformation, and samples were ellipsoidal in shape. This crystal orientation has two [111] slip directions, four {110} planes, and two {112} planes which have CRSS values of 0.41 and 0.47, respectively. The lower number of slip systems may have influenced the structure evolution at low and high strain rates.

The deformation in this orientation may be a combination of screws and edge dislocations as discussed by Herring (1992) and Leslie (1973). At low strain rates the screw components of the dislocations in BCC orientation crystals are able to cross-slip and generate dislocation networks and cell structures, while at high strain rate the screw components cannot cross-slip, and as a result, there is a lack of cell structure at high strain rate (Leslie 1973). This lack of cell structure at high strain rate may have allowed the load drop observed, after critical stress levels were reached to move dislocations by easy glide on the {110} or {112} planes. Consequently, since the structure at a particular strain may not be equivalent for low and high strain rates, the flow stresses behave anomalously, with lower stress at a higher strain rate for a given strain. However, the above mechanism has not been confirmed, and the specific mechanism which

may have caused the yield point and subsequent load drop for [110] and [111] crystals could not be determined from this set of experiments.

Leslie (1973) and others did observe that twinning in BCC iron and other single crystals was responsible for yield point effects. Also, the effect of interstitial solutes might need further investigation, since various researchers, Cottrell (1953) for one, have indicated the sensitivity of the shape of BCC single-crystal flow curves to interstitial impurities. Further, if the theoretical shear stress vs. shear strain curves for various orientation crystals, [110], [111], and [100] (see Figure 39 after Dieter 1986) are compared with the experimental results (see Figures 29–31), it might be observed that the general shape of the experimental curves is consistent with theory, if the yield points are ignored. This would possibly lend additional support to interstitial impurities, or twinning effecting the shape of the curves for lower symmetry orientation crystals [110] and [111]. However, evidence of twinning was not seen in [110] or [111] tungsten crystals subjected to high-rate loading during ballistic test (Herring 1992).

For the [111] crystal orientation, samples after test appeared to have numerous slip planes evident on the surface, with a large-scale slip and small-scale microslip structure mixed (see Figures 34 and 35). Also, samples after test appeared to have an hourglass-type shape, which would seem quite unexpected compared to the normal barrelled-type shape after compression test. For this crystal orientation, there are three symmetric [111] slip directions at 60°. There are four {110} and two {112} planes available with CRSS of 0.27 and 0.30, respectively. Also, the CRSS factor for the stress component of pure screw dislocations is only cos(70.5) or 0.33.

It is believed that the dominant deformation mechanism was that proposed by Weertman and Weertman (1965) and Herring (1992), where pure screw dislocations dominate the deformation. Since the (111) orientation has a screw dislocation with stress component normal to the penetrator axis and since this orientation has CRSS = 1, this orientation is very favorable for generation of screws and material flow using the vertical/horizontal set of screws type process mentioned previously after Weertman and Weertman. A combination of this dislocation motion and some dislocation movement on other planes with lower CRSS would most likely produce the type of behavior seen in Kolsky bar compression test (hourglass shape). The yield point load drop may be the result of interstitial impurities and/or twinning of the microstructure.

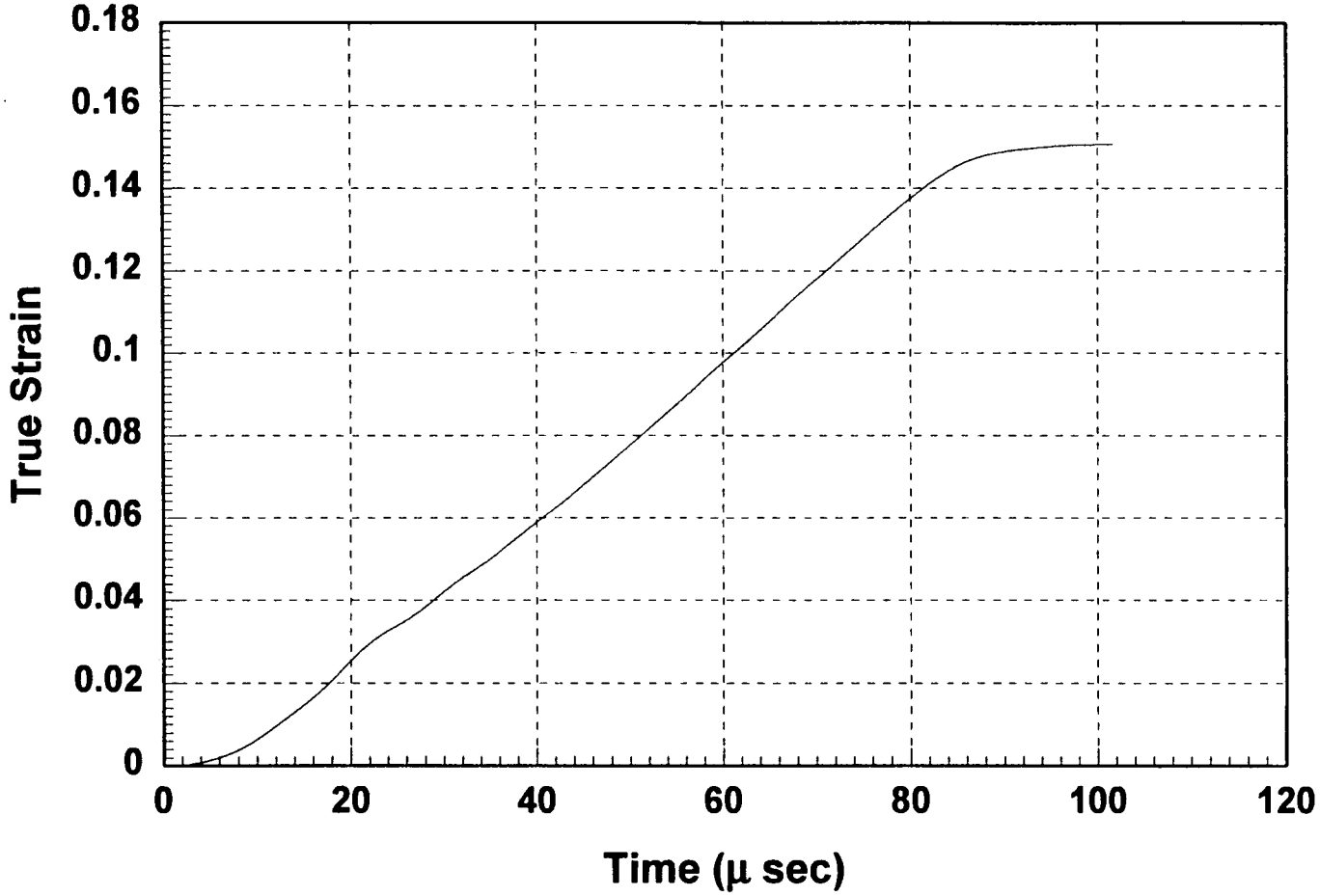

Figure 1. True strain vs. time - [100] tungsten single crystal no. 1.

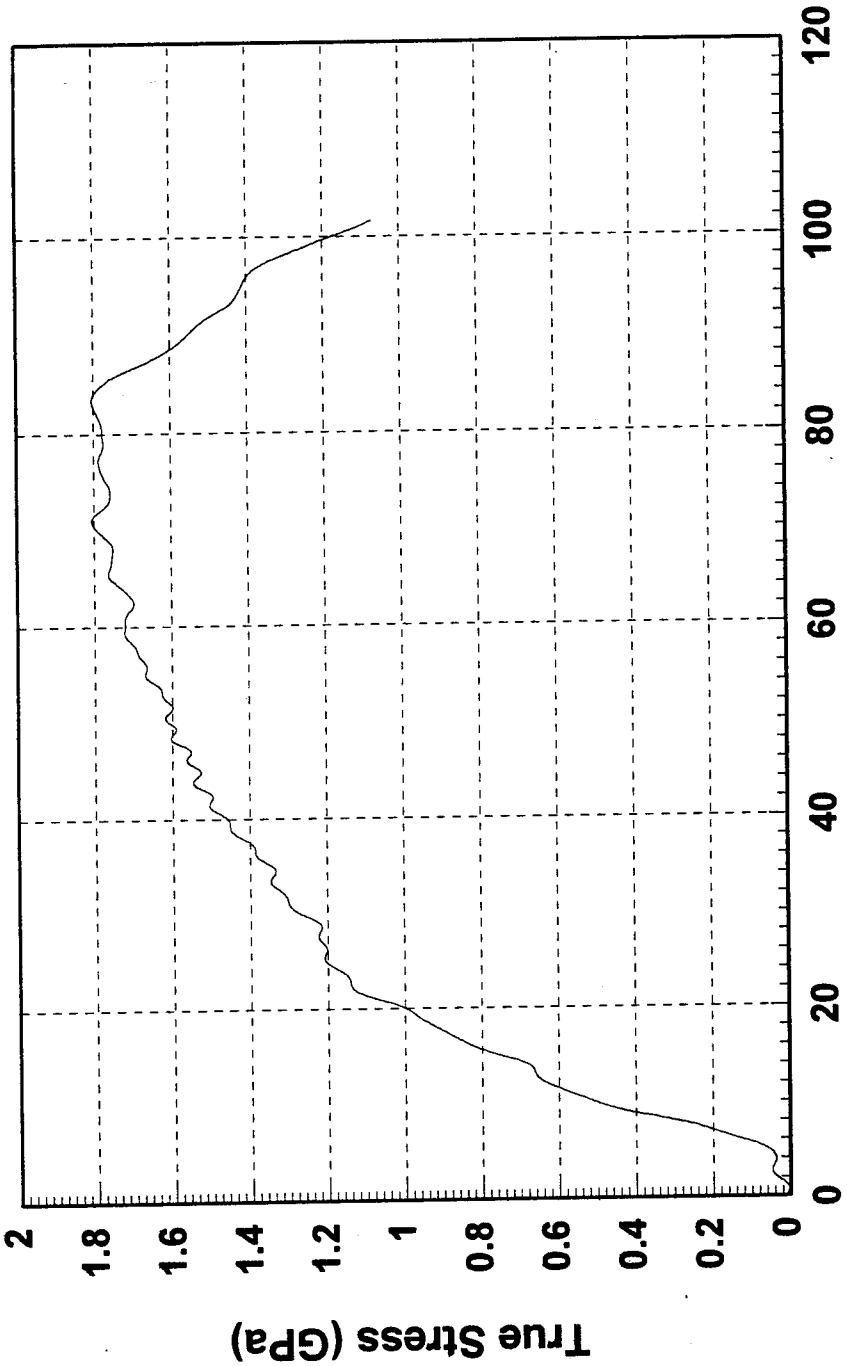

Figure 2. True stress vs. time - [100] tungsten single crystal no. 1.

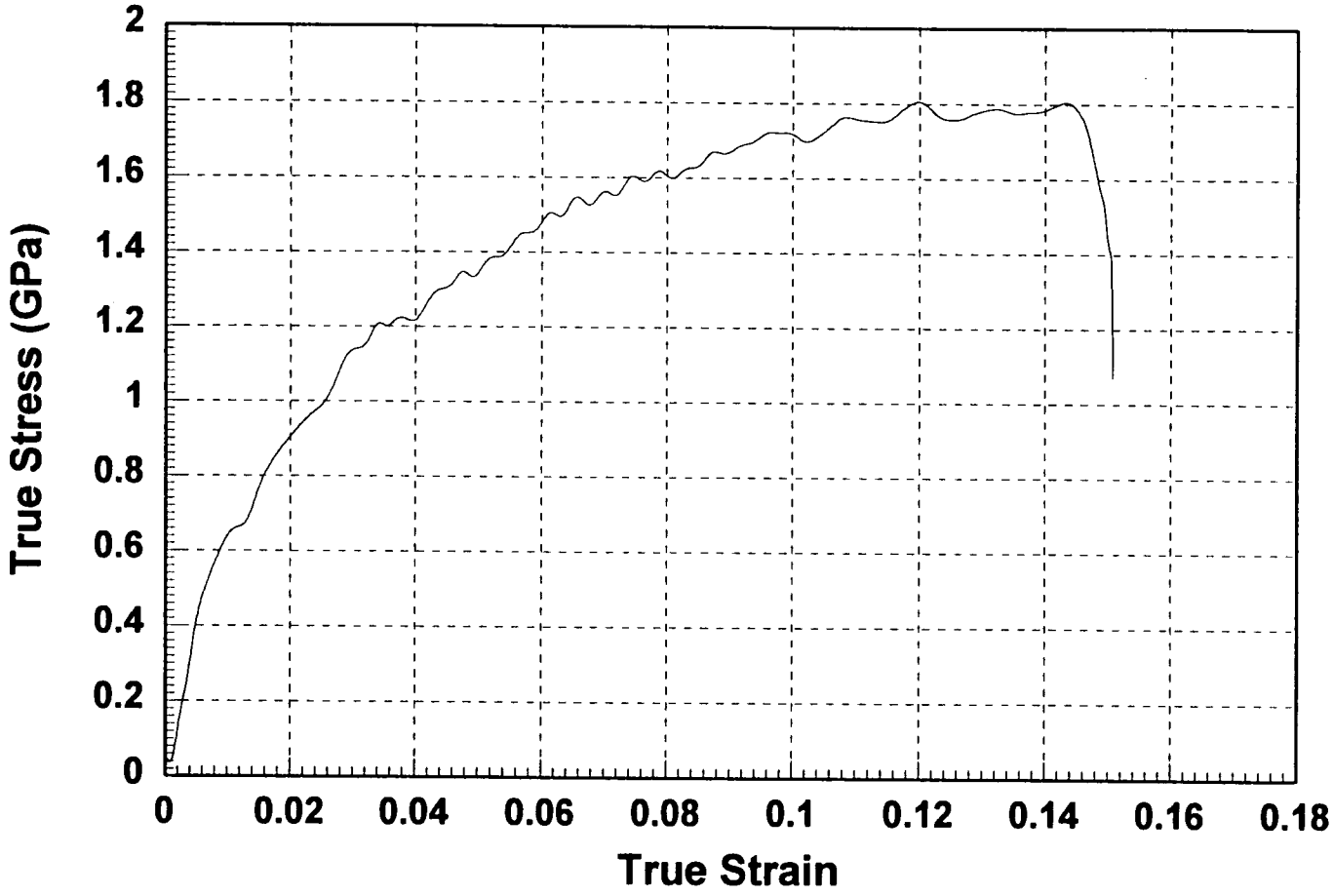

Figure 3. True stress vs. true strain - [100] tungsten single crystal no. 1.

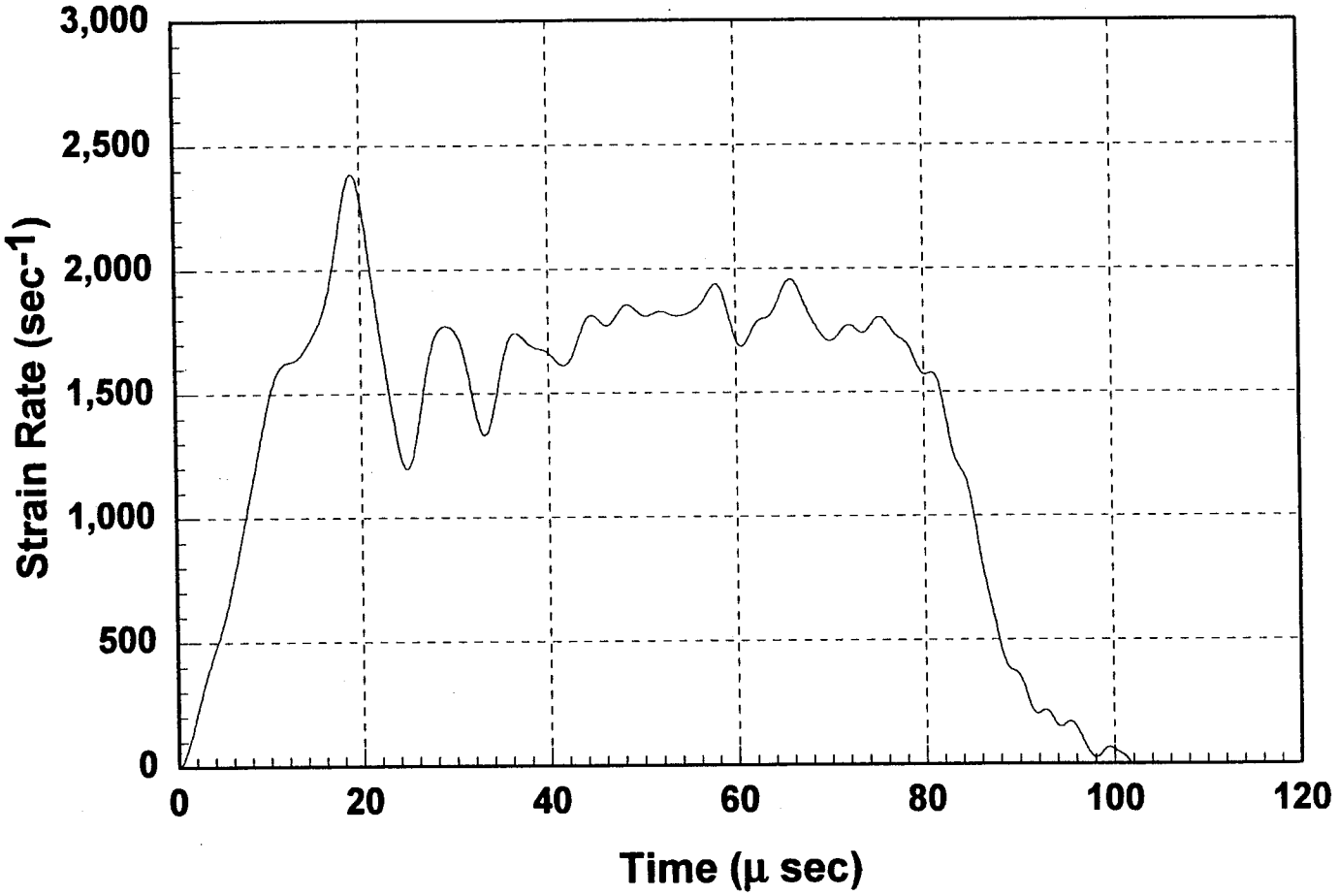

Figure 4. Strain rate vs. time - [100] tungsten single crystal no. 1.

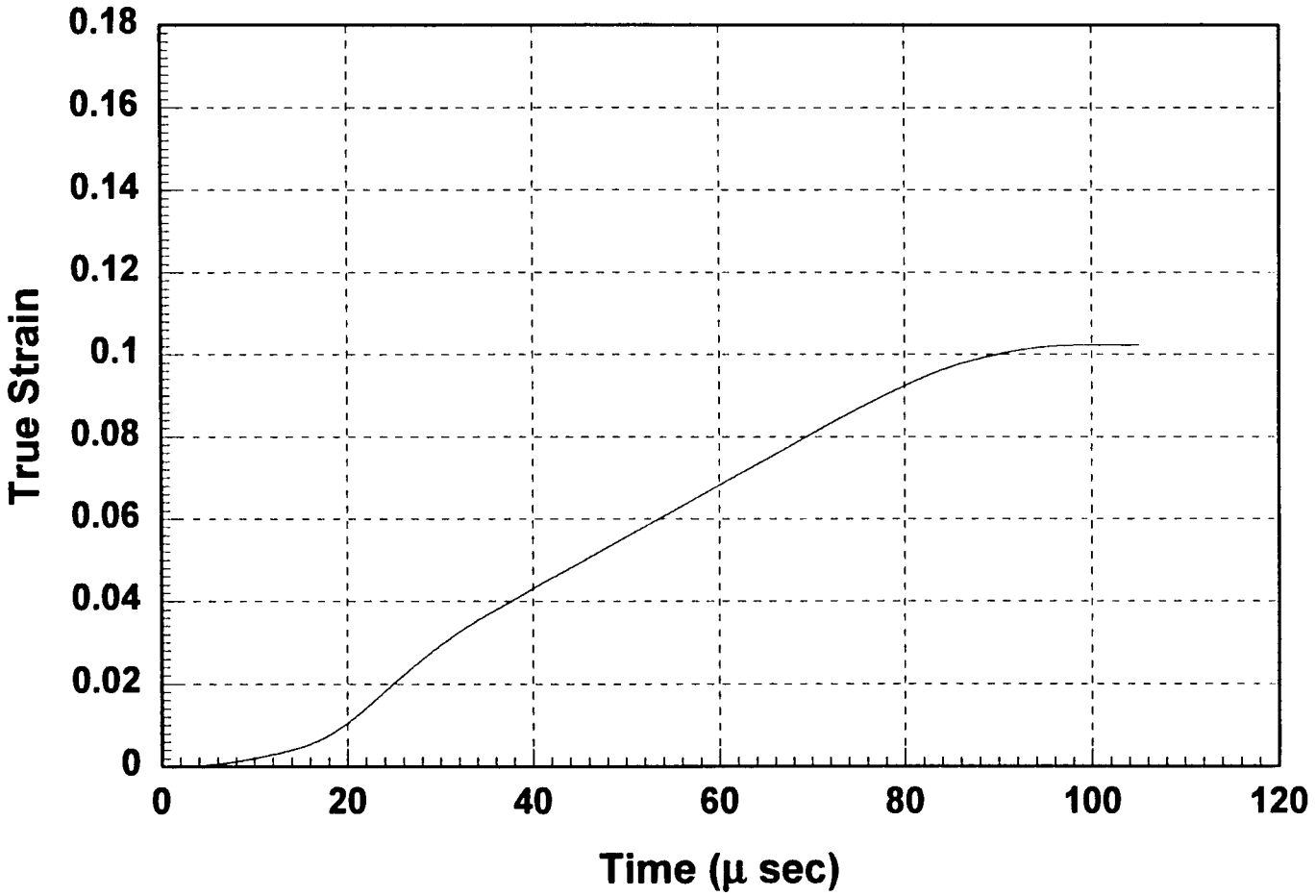

Figure 5. True strain vs. time - [100] tungsten single crystal no. 2.

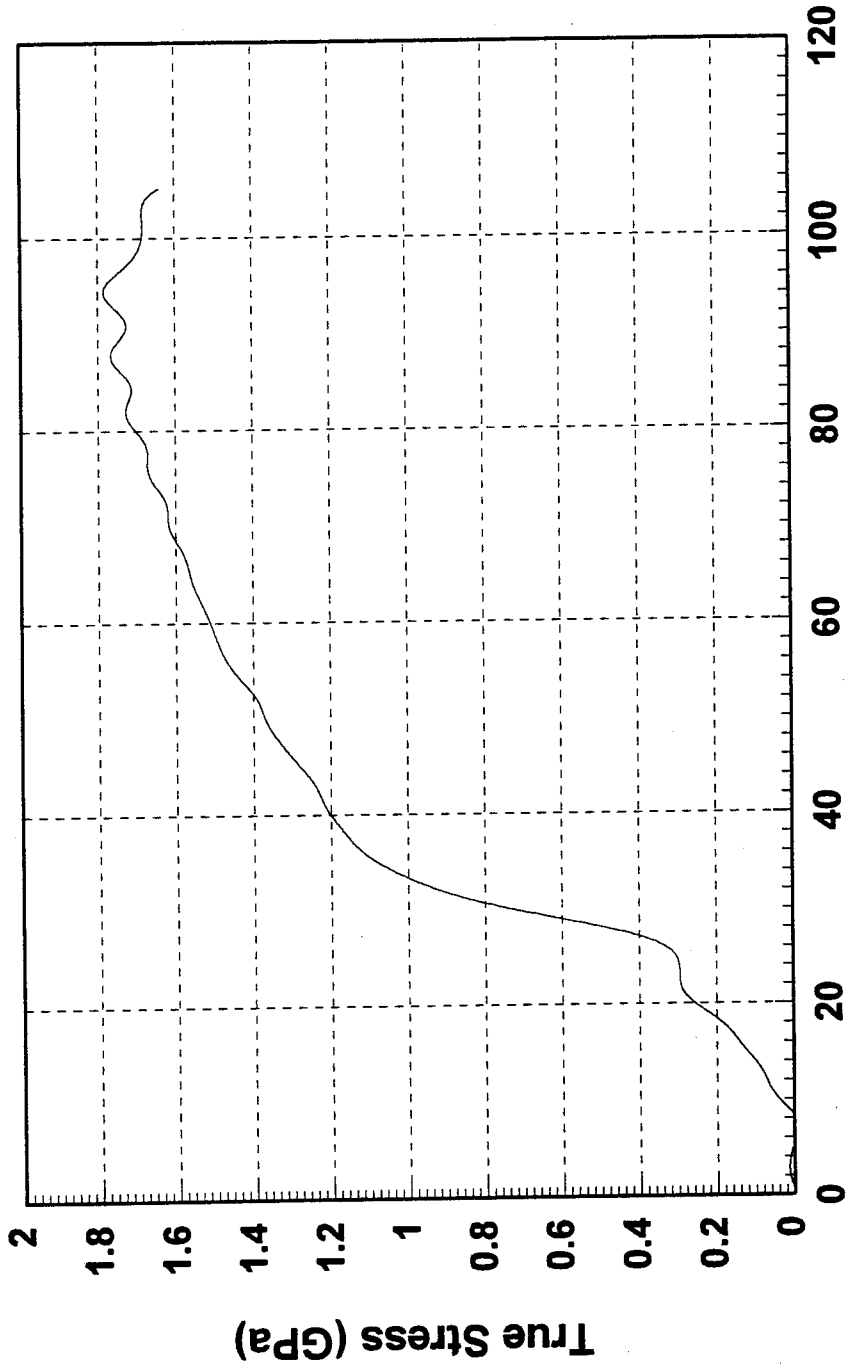

Figure 6. True stress vs. time - [100] tungsten single crystal no. 2.

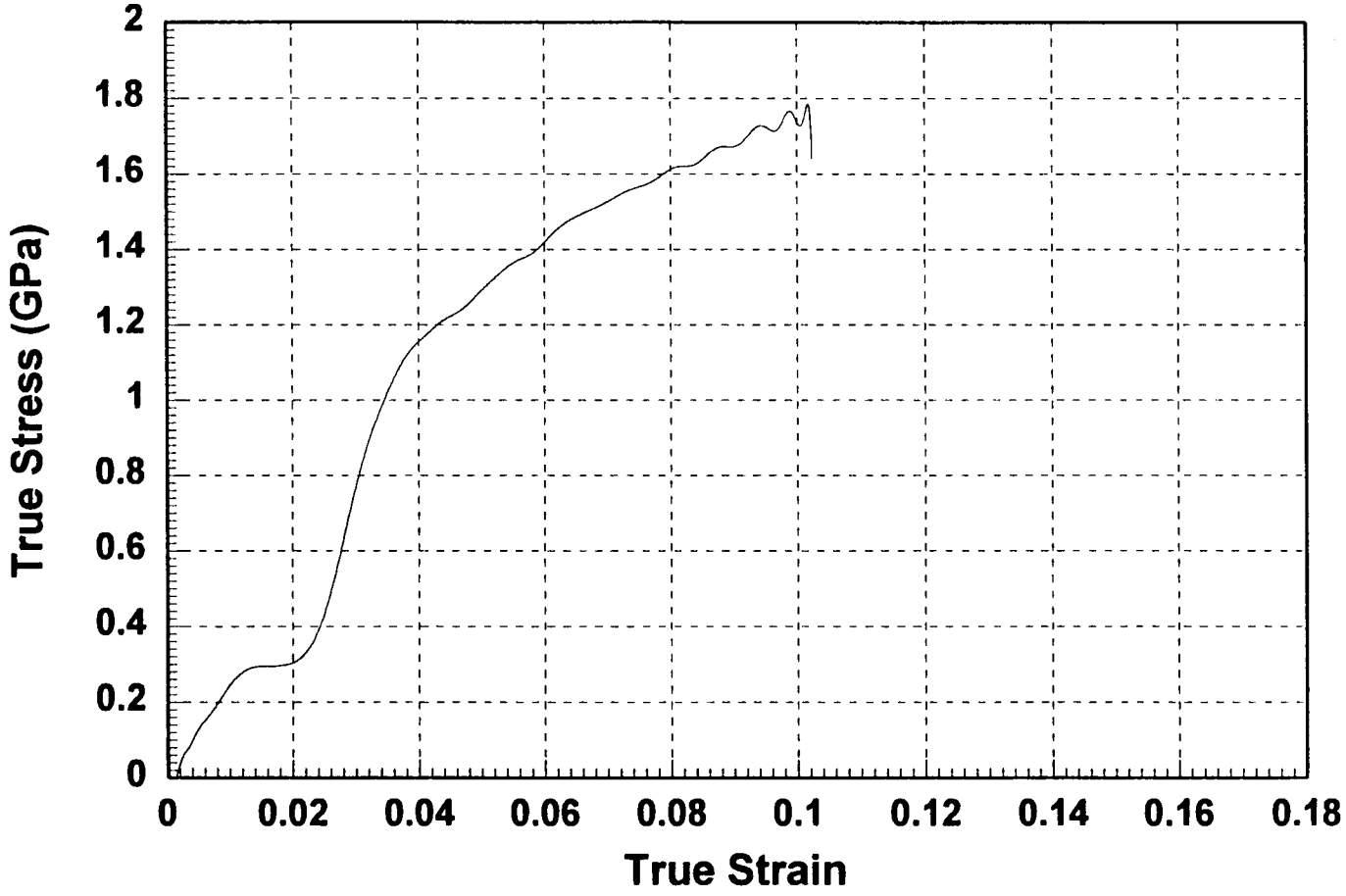

Figure 7. True stress vs. true strain - [100] tungsten single crystal no. 2.

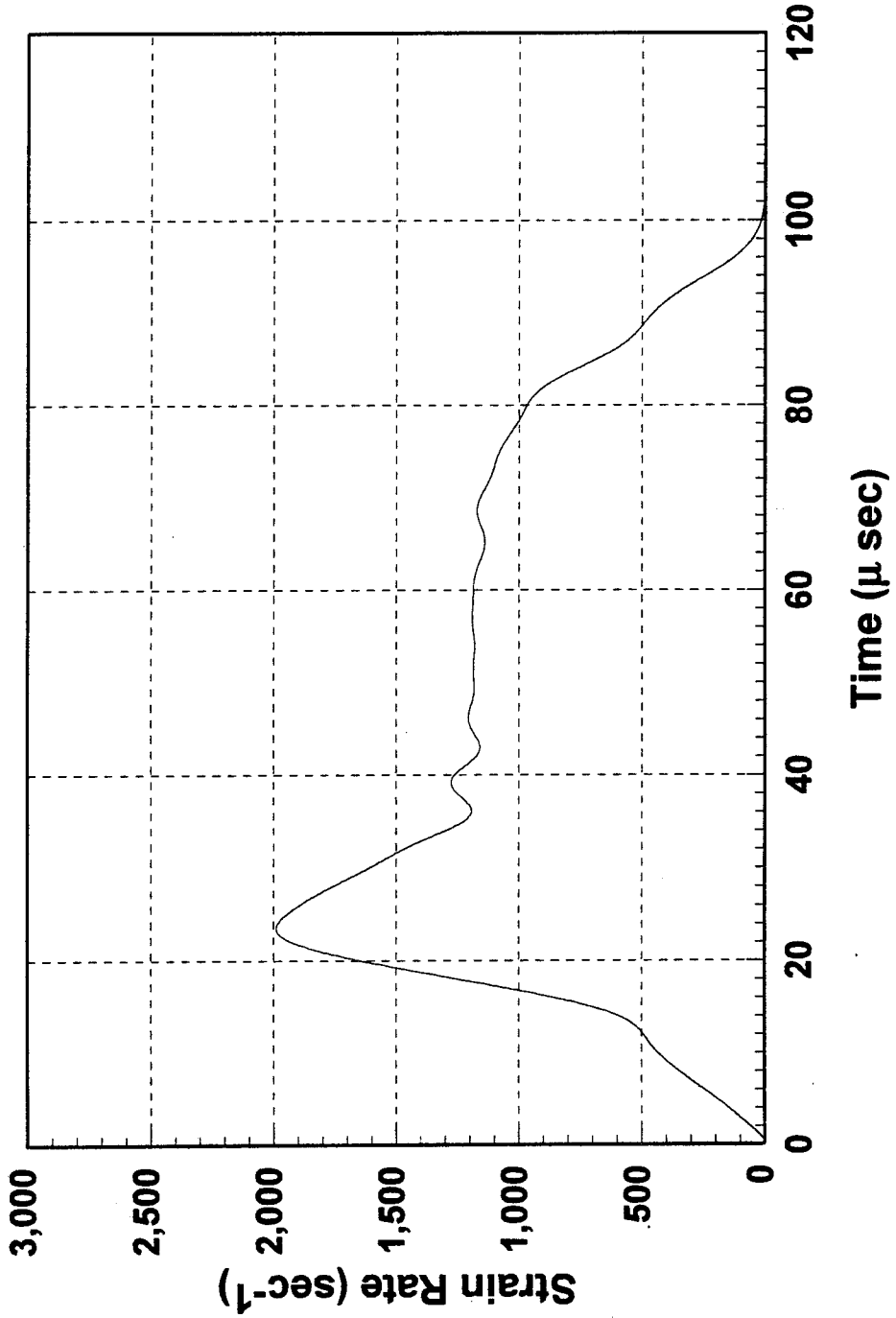

Figure 8. Strain rate vs. time - [100] tungsten single crystal no. 2.

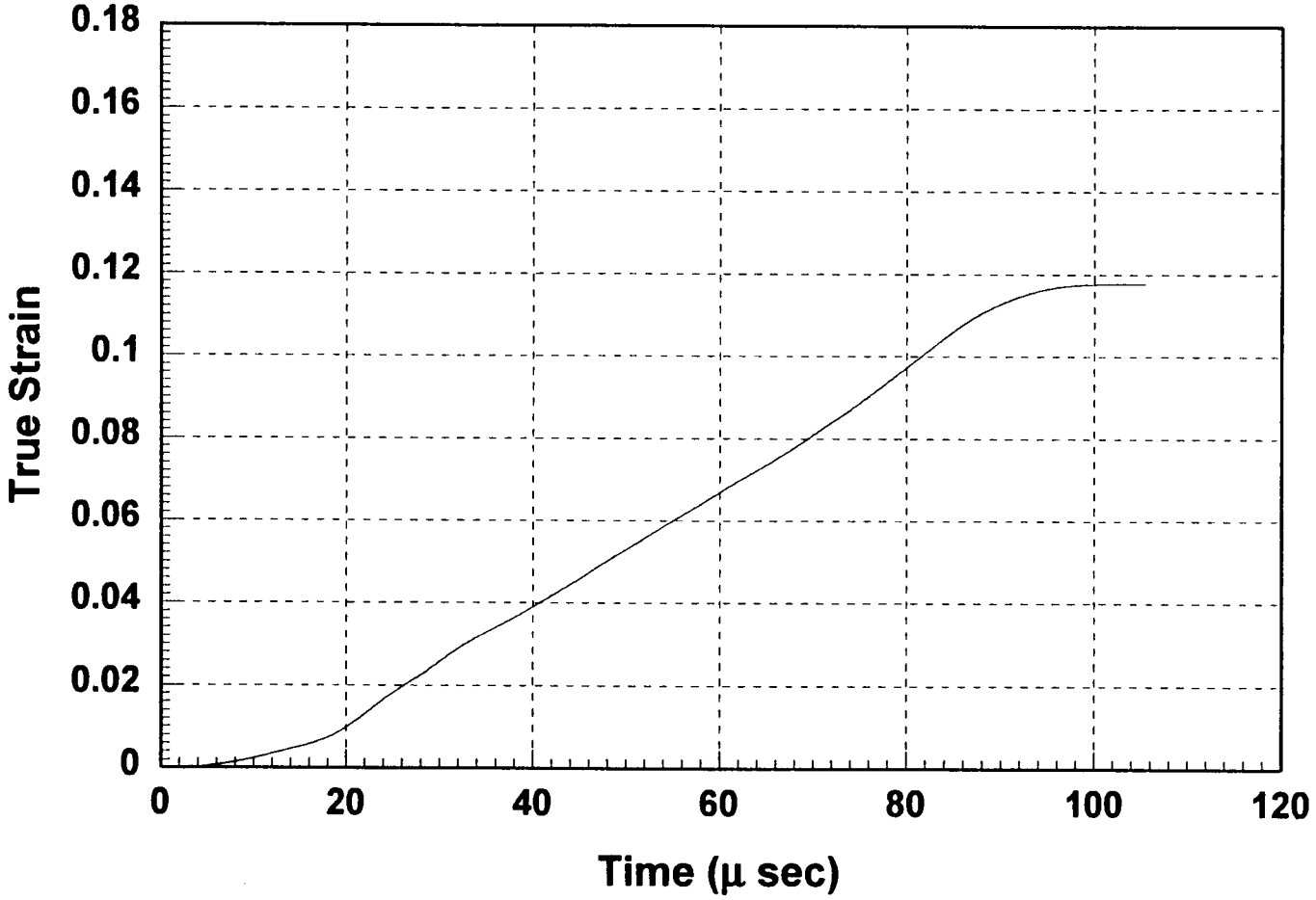

Figure 9. True strain vs. time - [111] tungsten single crystal no. 1.

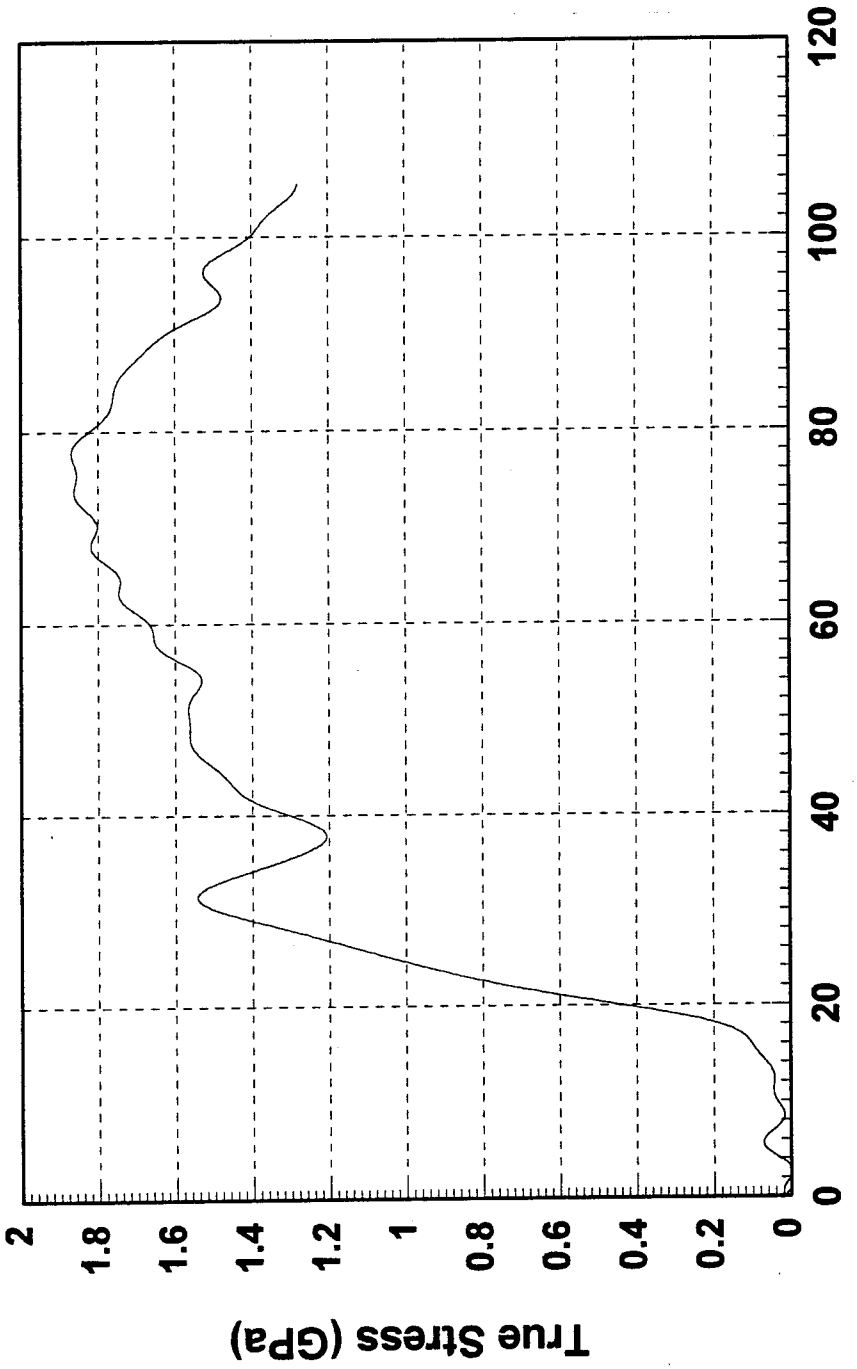

Figure 10. True stress vs. time - [111] tungsten single crystal no. 1.

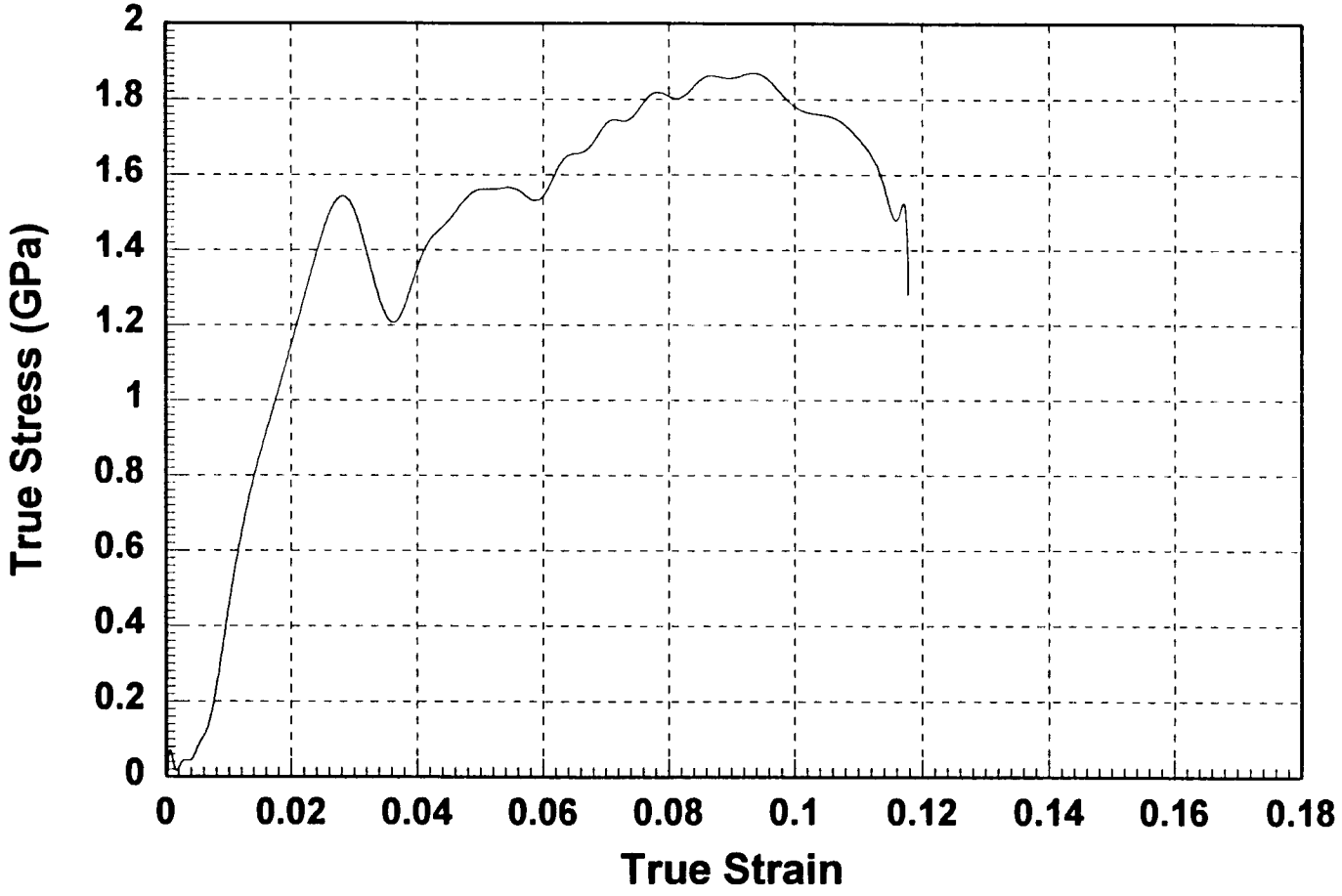

Figure 11. True stress vs. true strain - [111] tungsten single crystal no. 1.

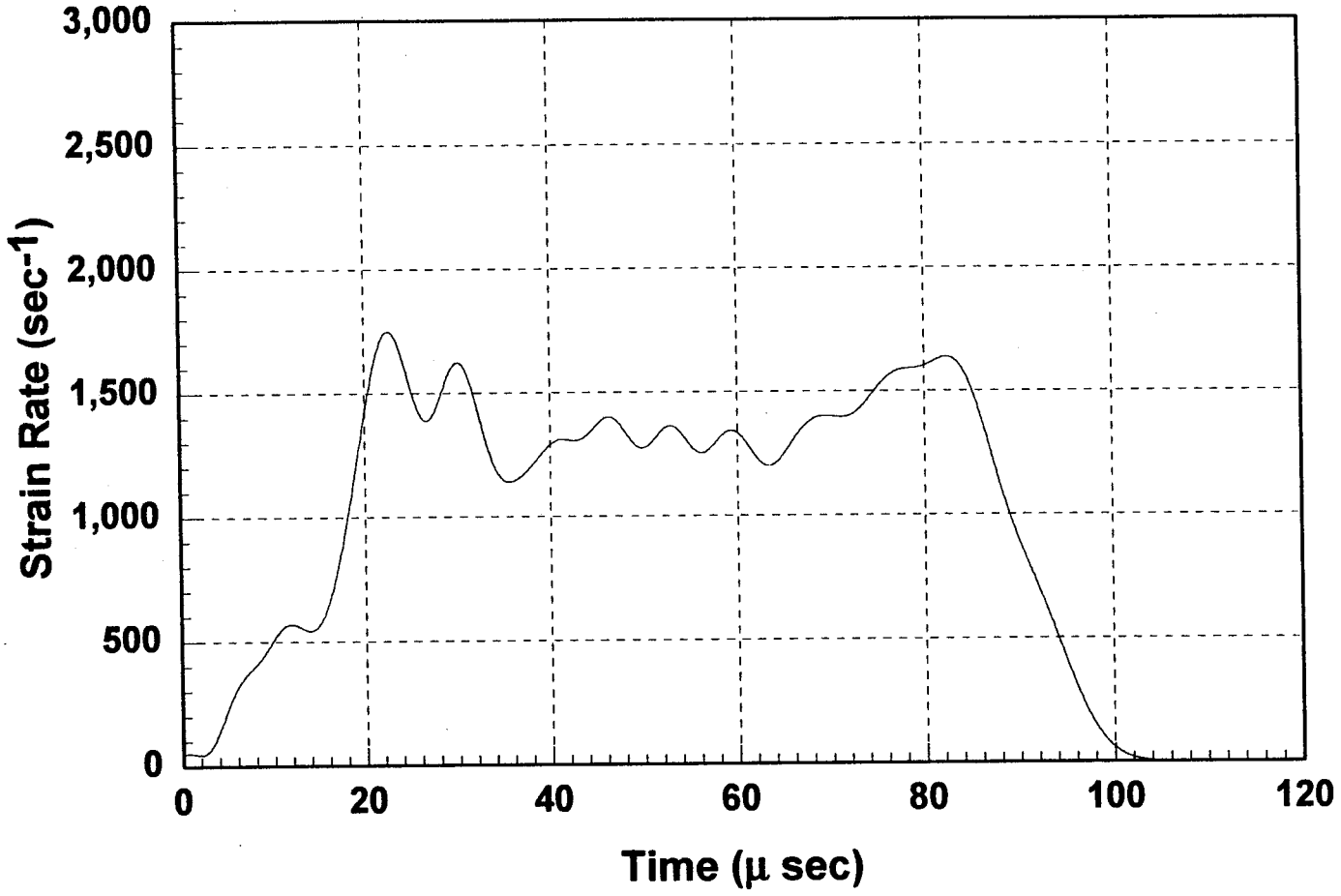

Figure 12. Strain rate vs. time - [111] tungsten single crystal no. 1.

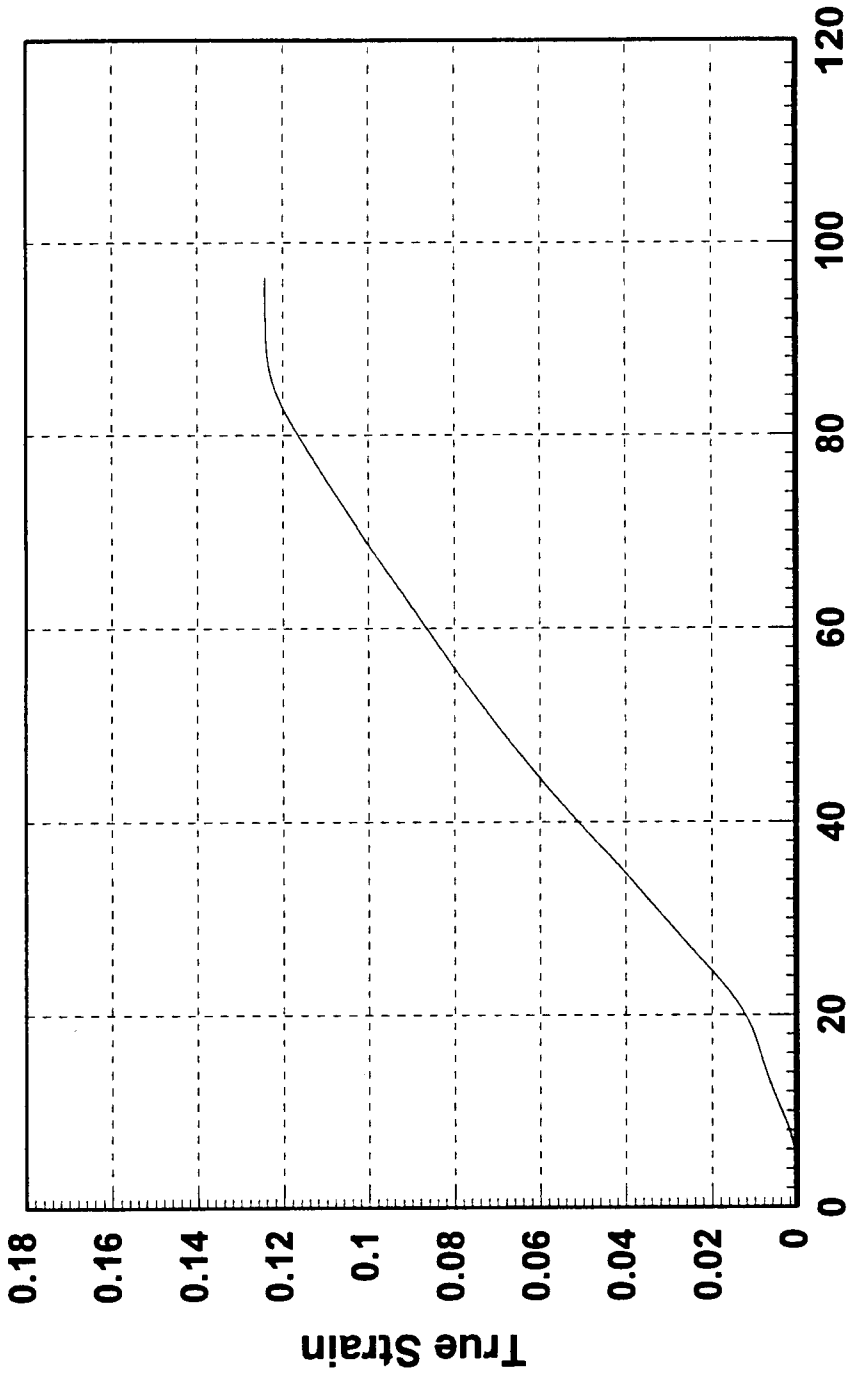

Figure 13. True strain vs. time - [111] tungsten single crystal no. 2.

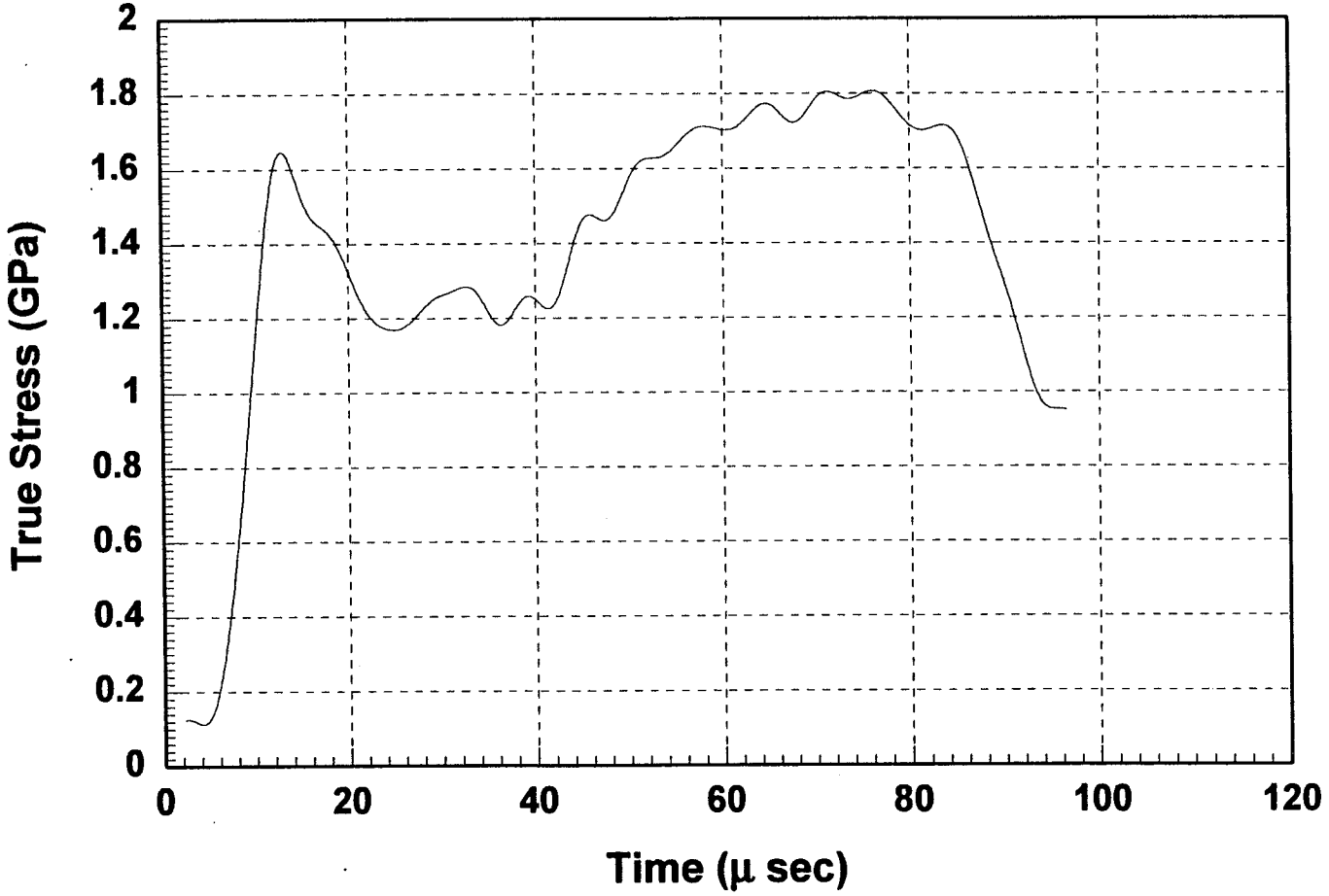

Figure 14. True stress vs. time - [111] tungsten single crystal no. 2.

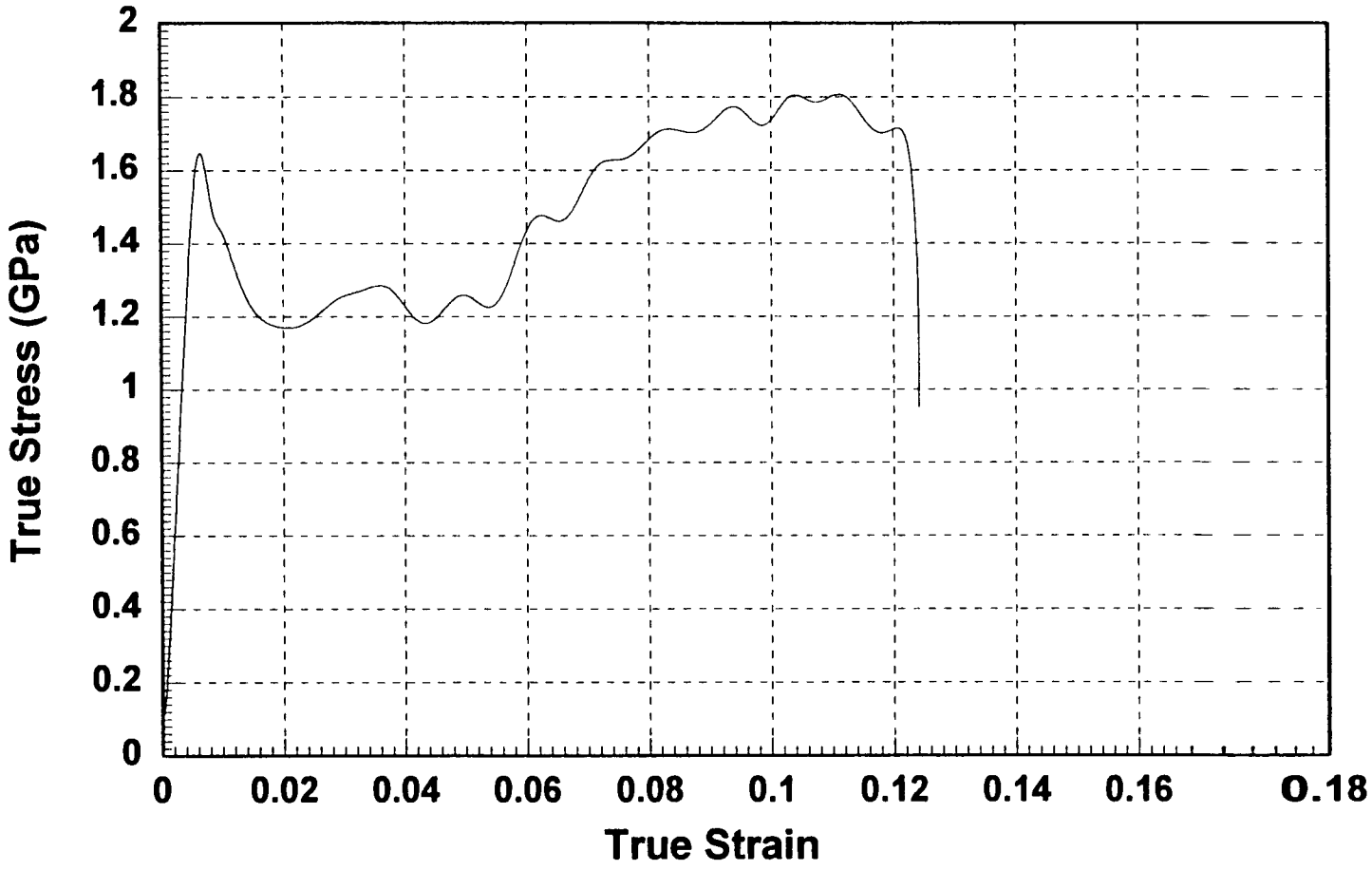

Figure 15. True stress vs. true strain - [111] tungsten single crystal no. 2.

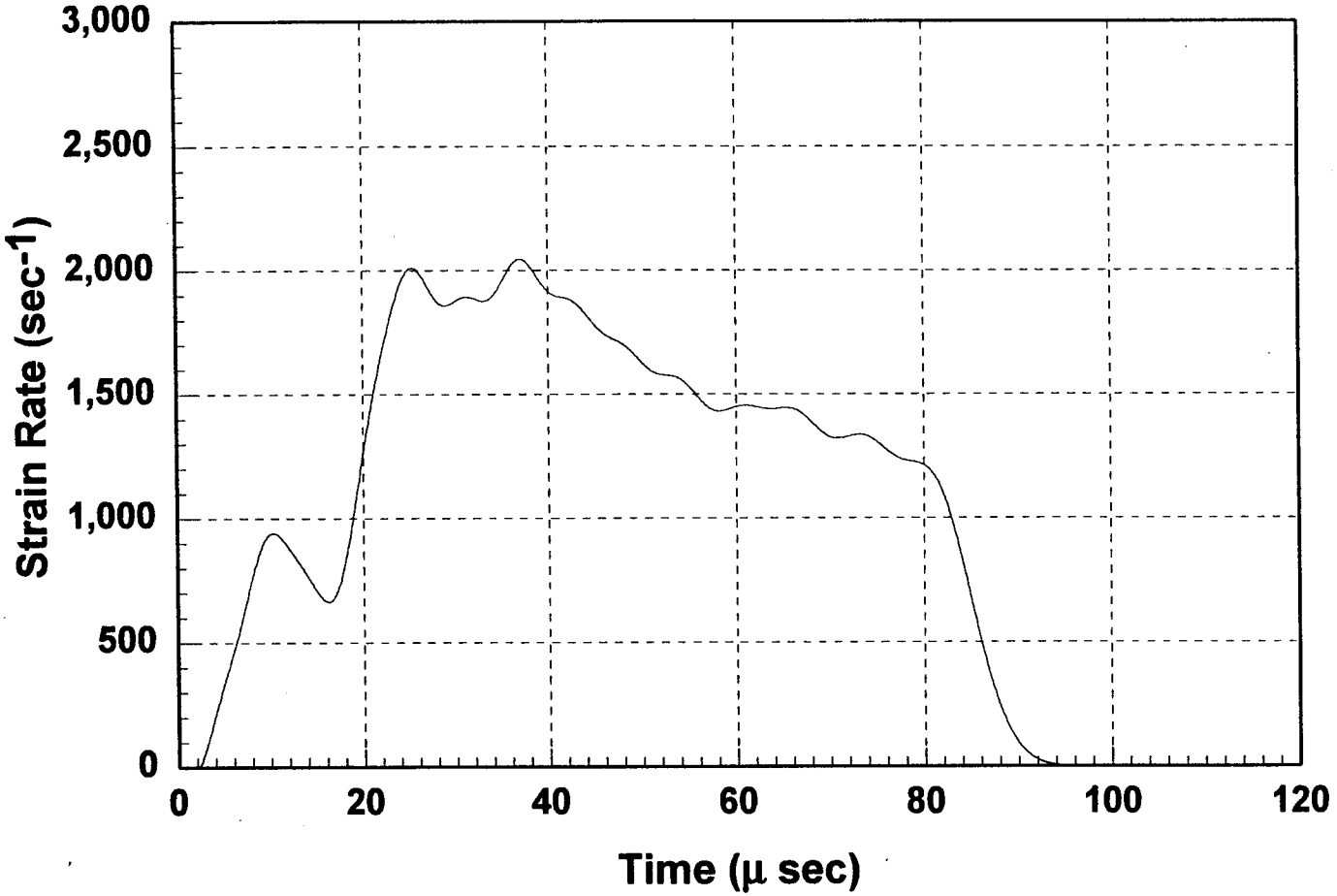

Figure 16. Strain rate vs. time - [111] tungsten single crystal no. 2.

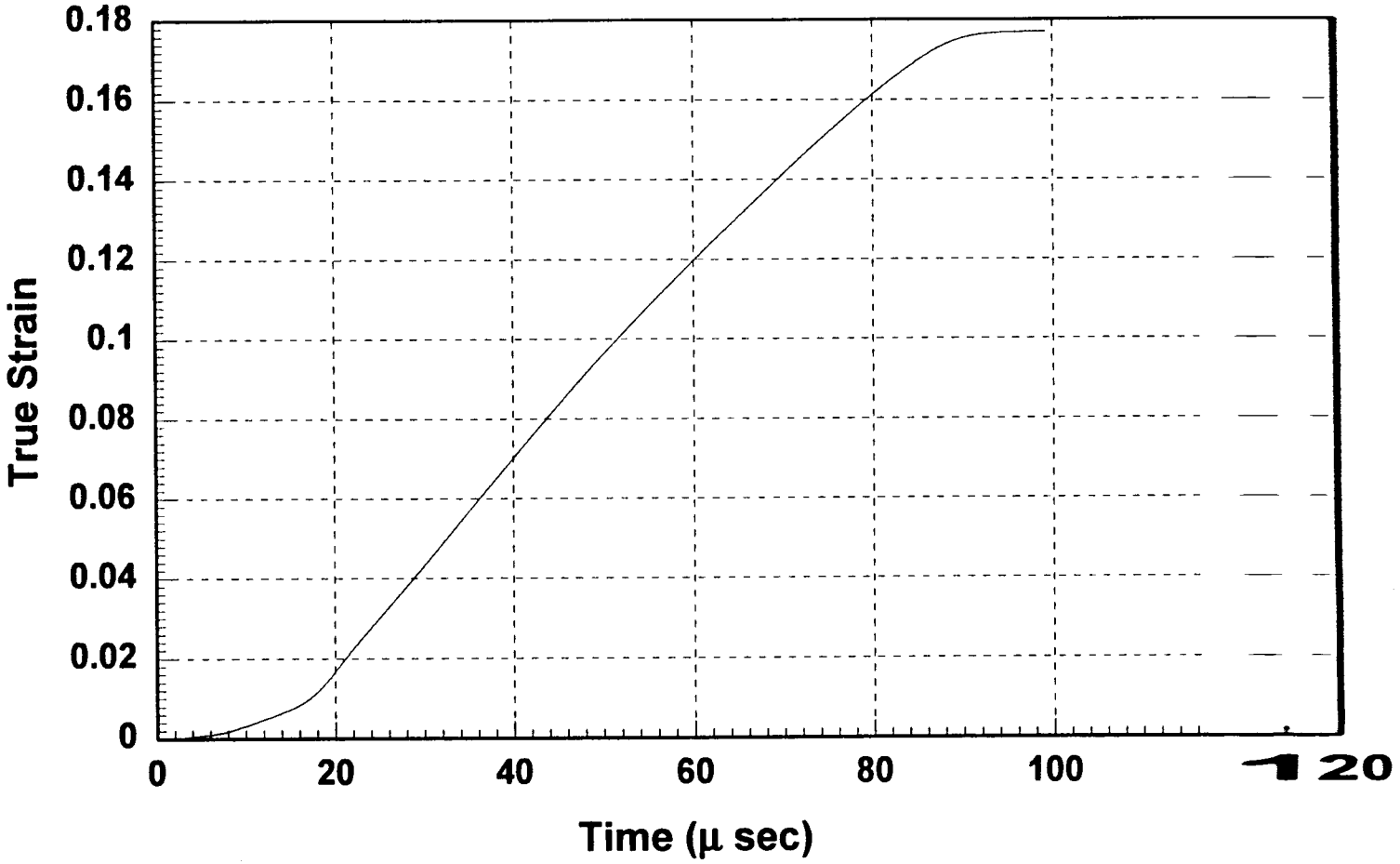

Figure 17. True strain vs. time - [110] tungsten single crystal no. 1.

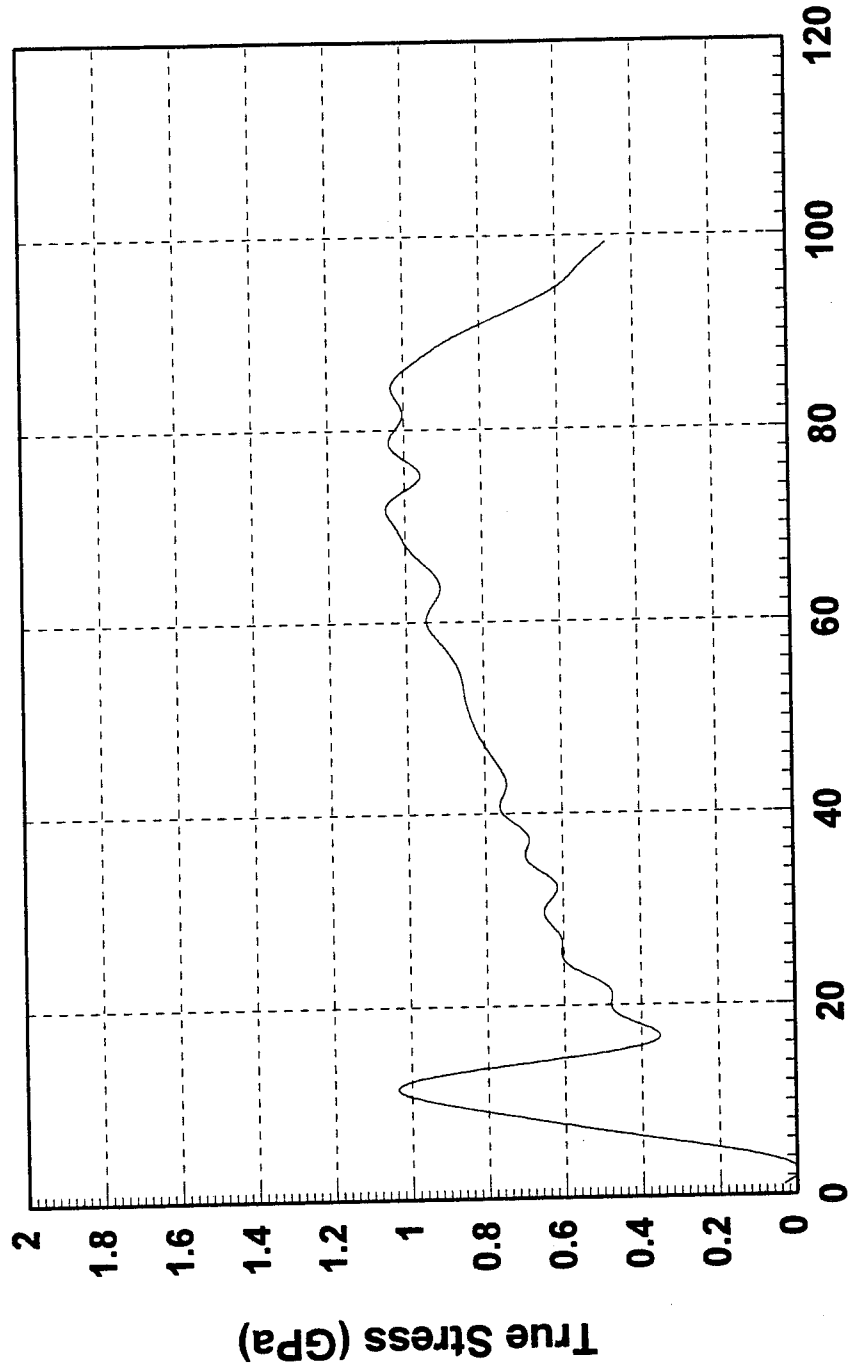

Figure 18. True stress vs. time - [110] tungsten single crystal no. 1.

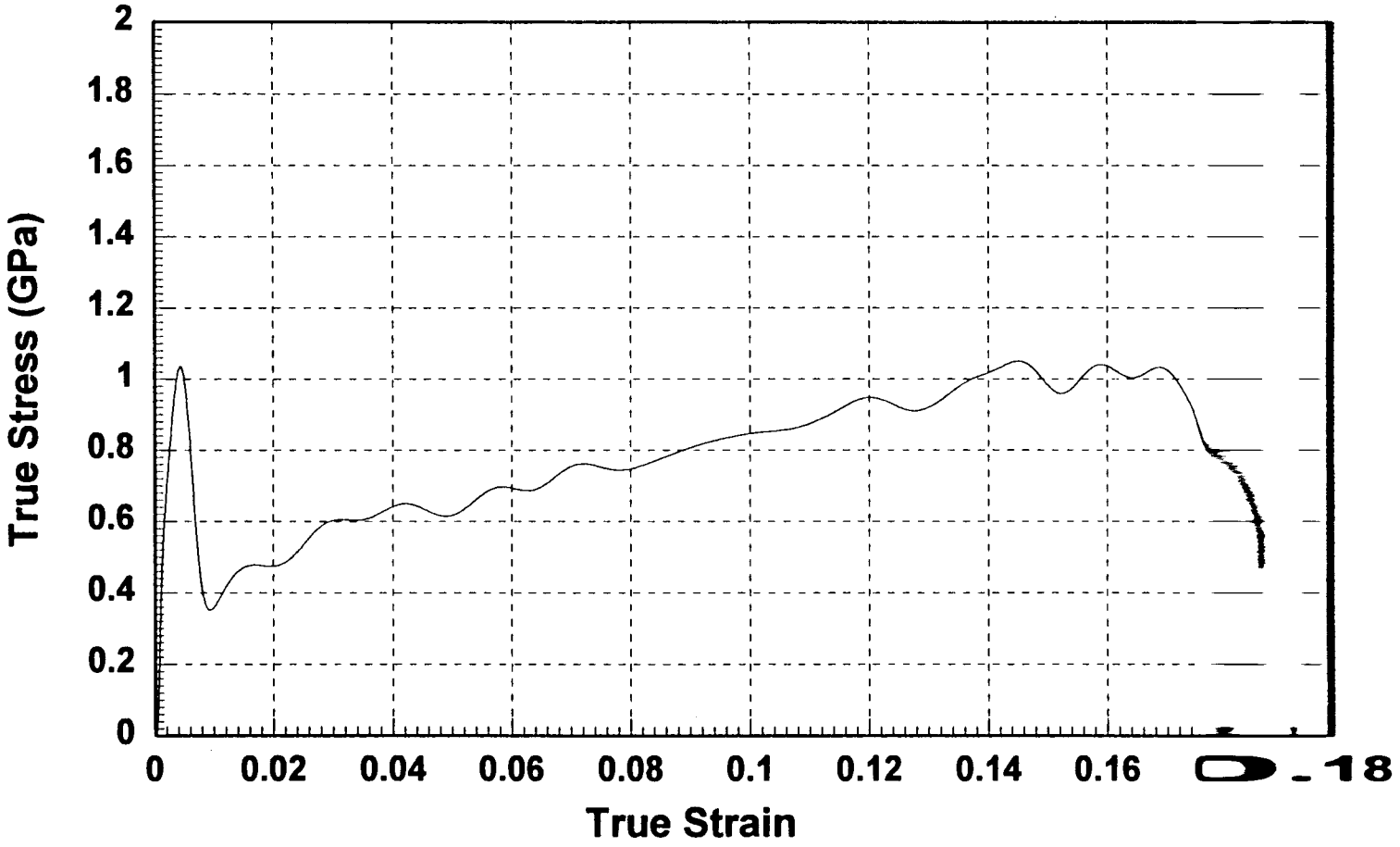

Figure 19. True stress vs. true strain - [110] tungsten single crystal no. 1.

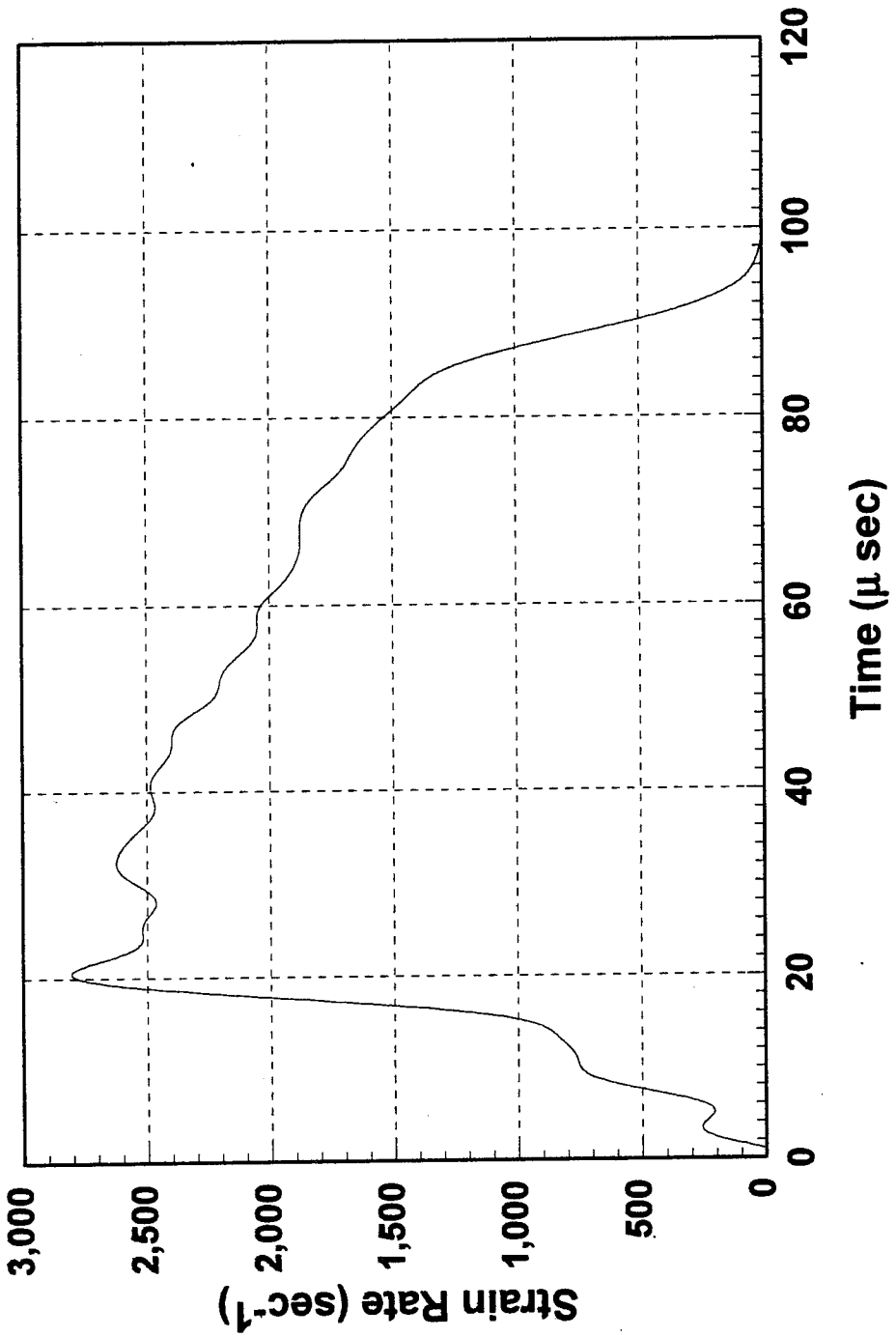

Figure 20. Strain rate vs. time - [110] tungsten single crystal no. 1.

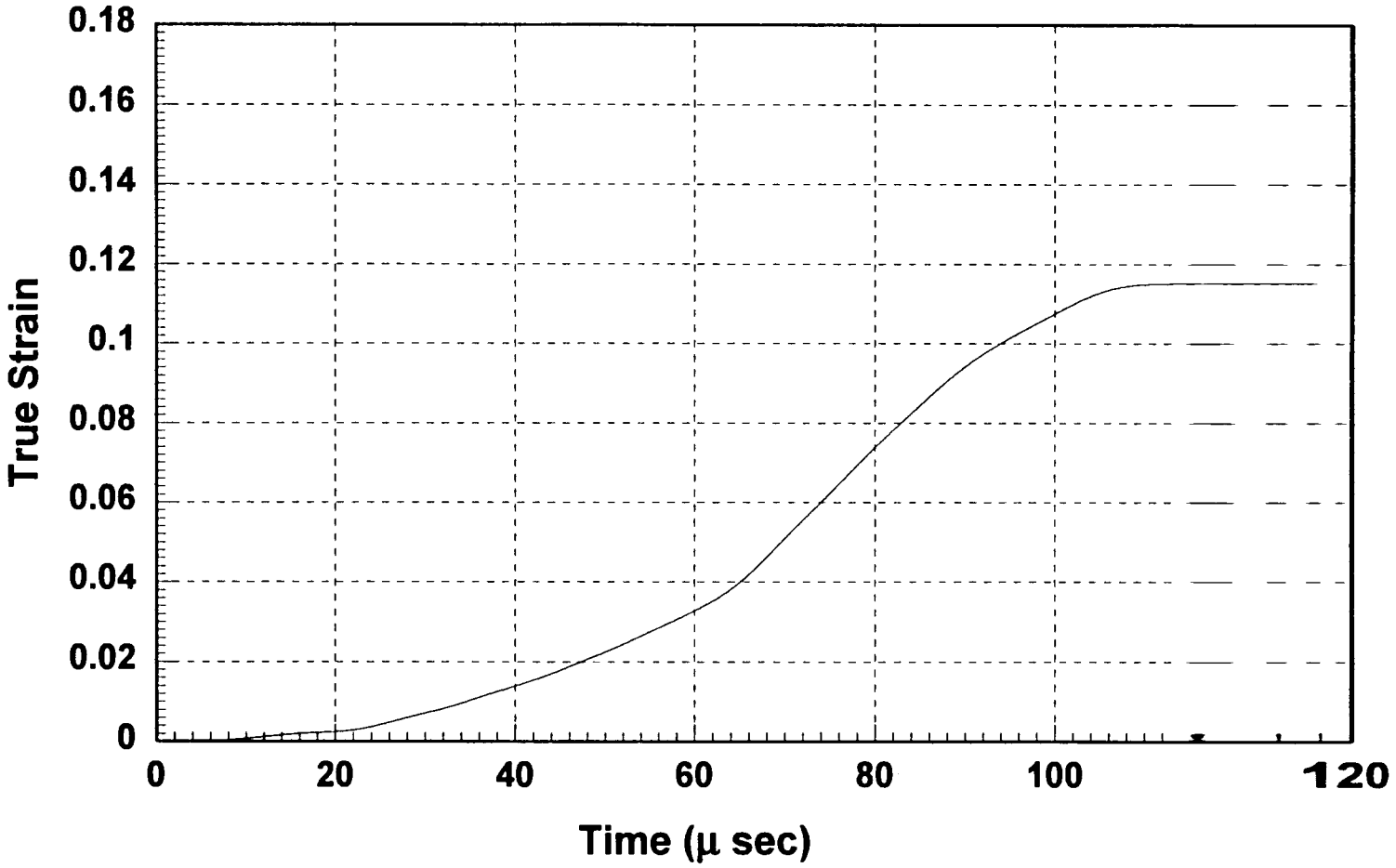

Figure 21. True strain vs. time - [110] tungsten single crystal no. 2.

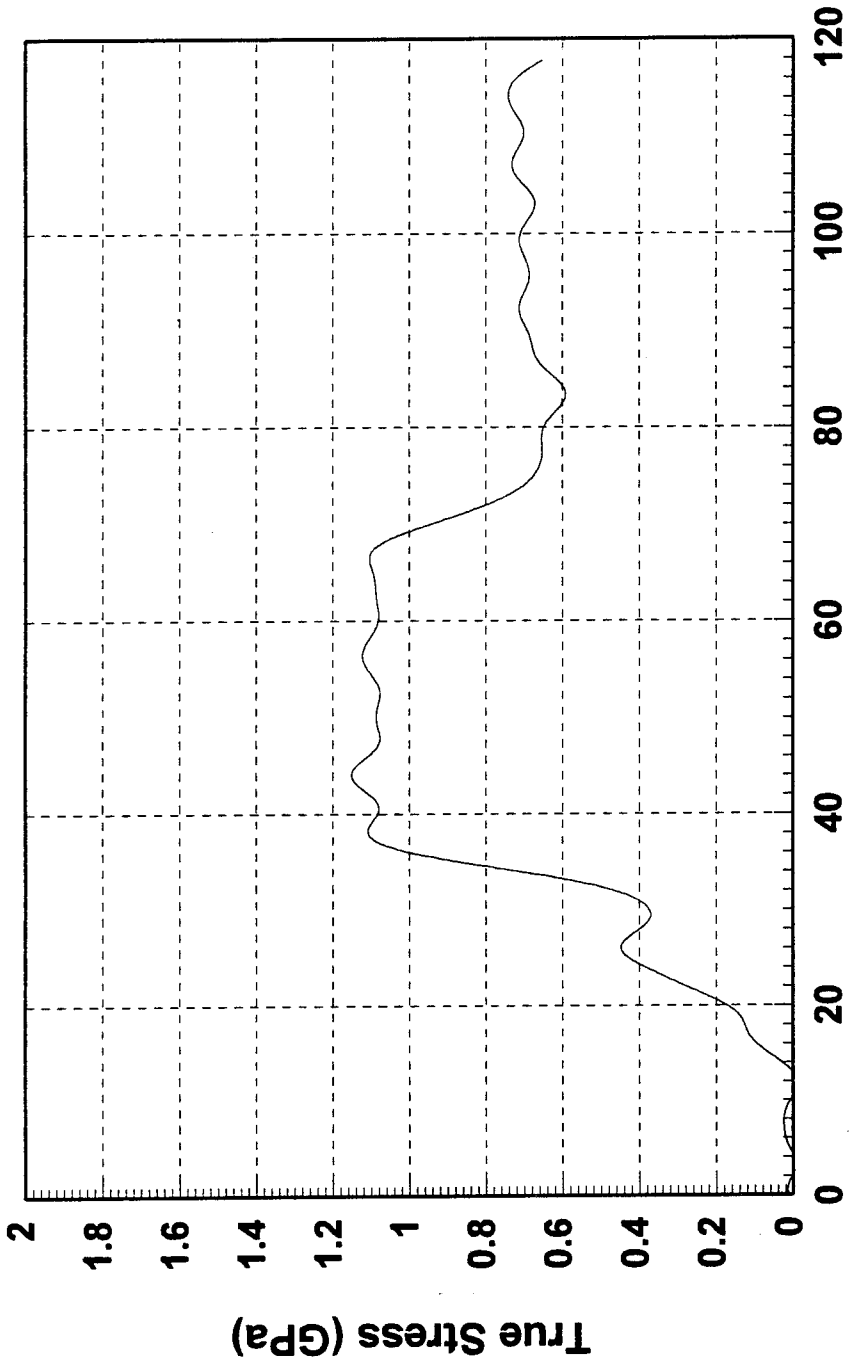

Figure 22. True stress vs. time - [110] tungsten single crystal no. 2.

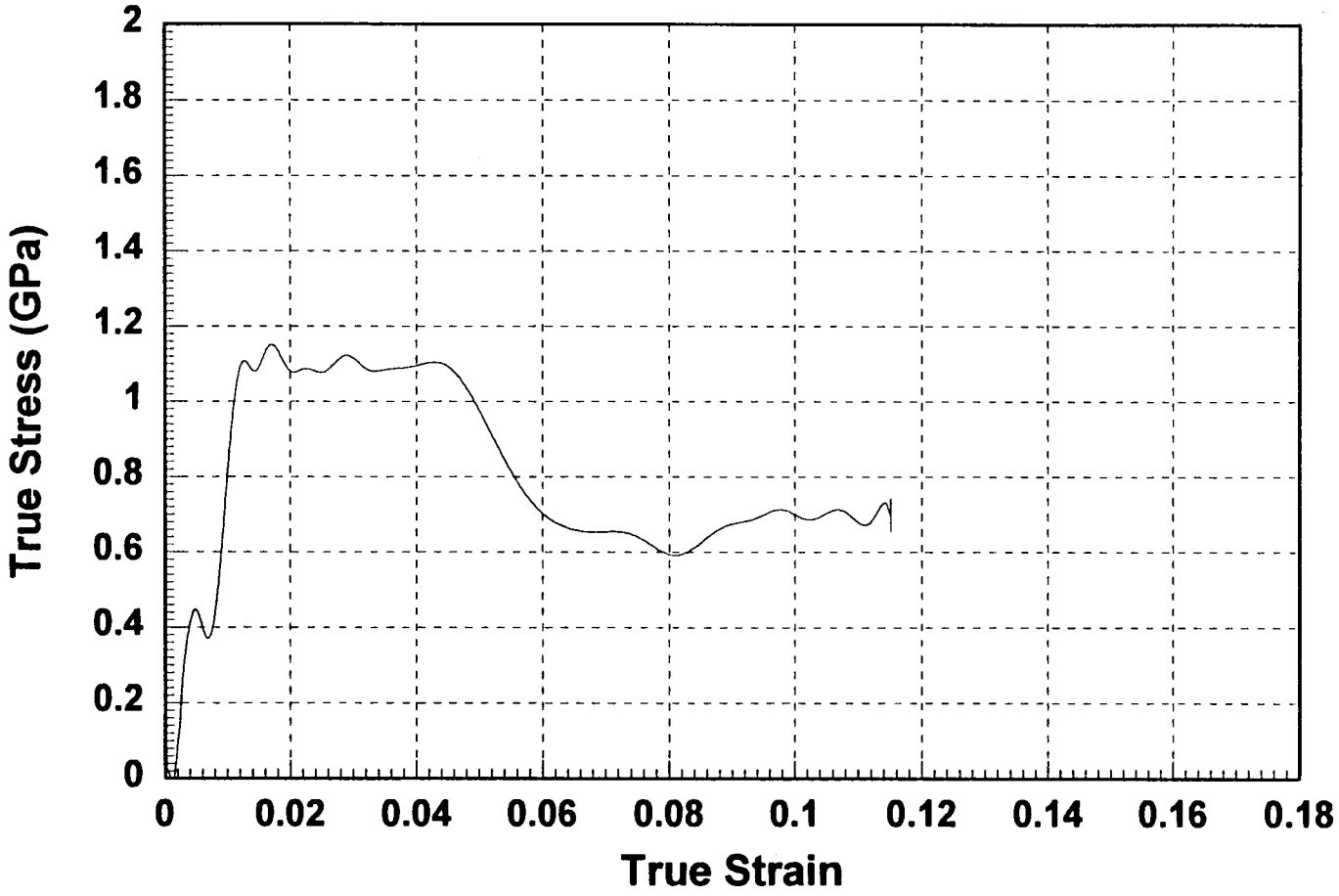

Figure 23. True stress vs. true strain - [110] tungsten single crystal no. 2.

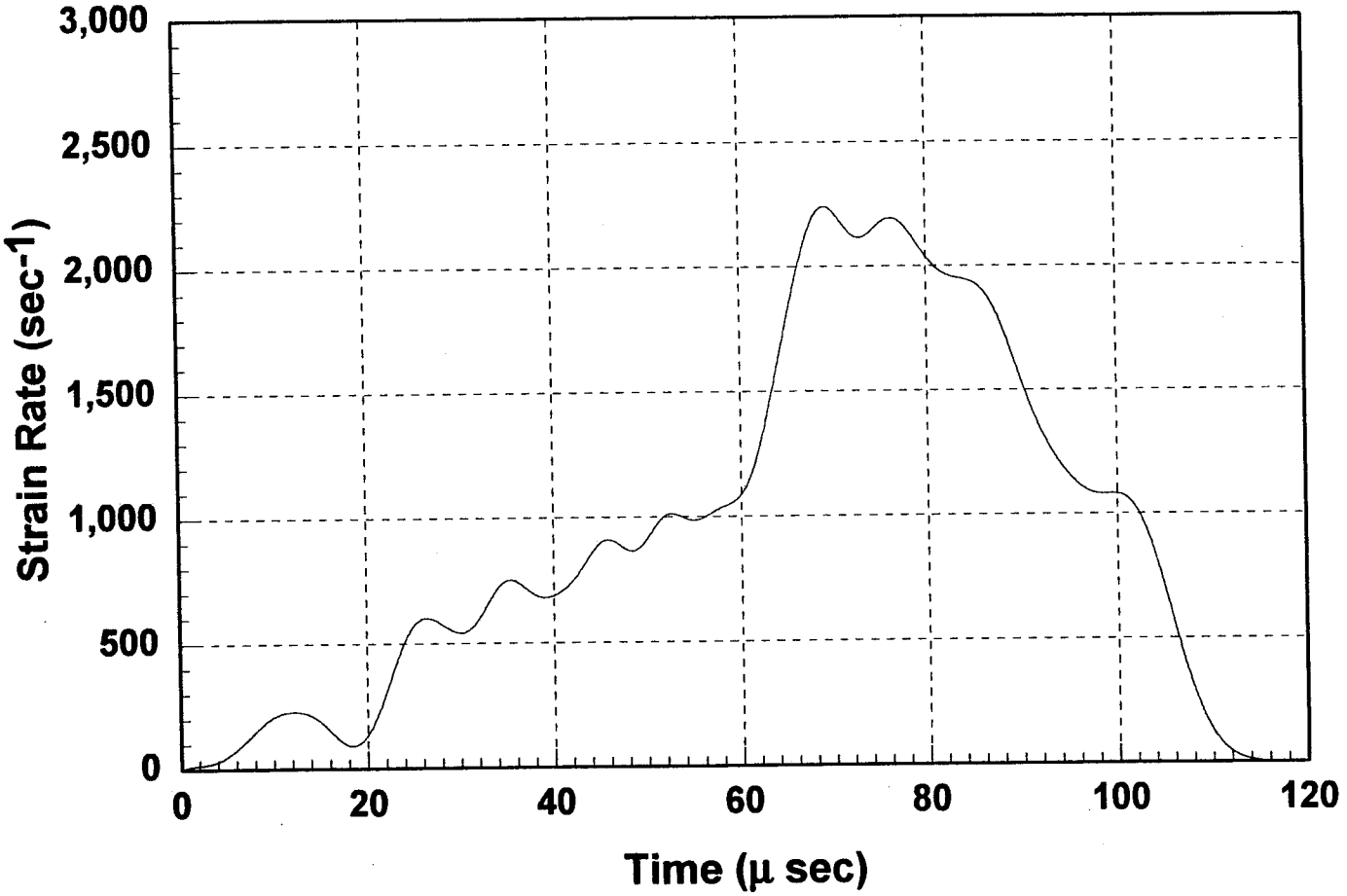

Figure 24. Strain rate vs. time - [110] tungsten single crystal no. 2.

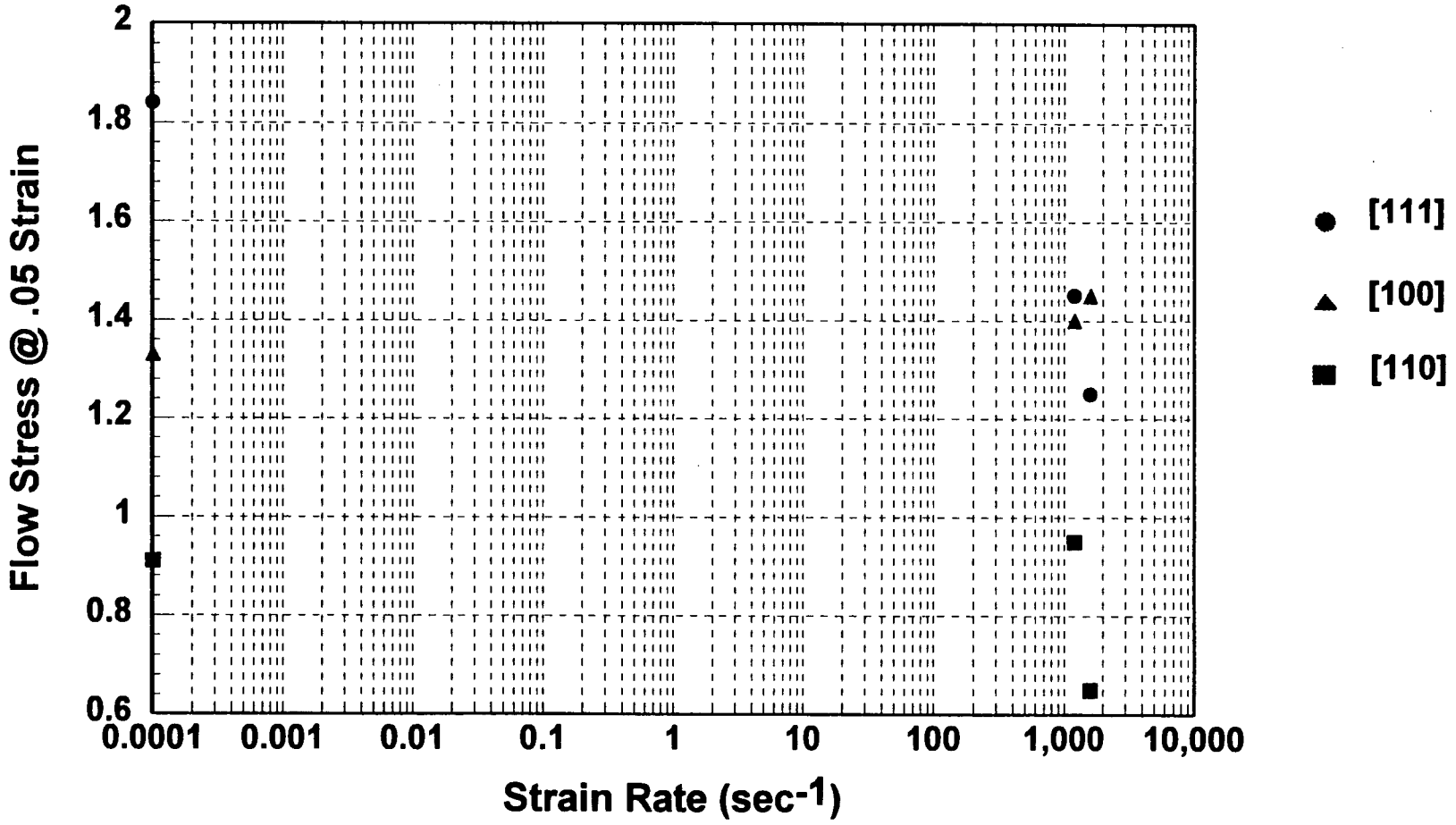

Figure 25. Flow stress (at .05 strain) vs. strain rate.

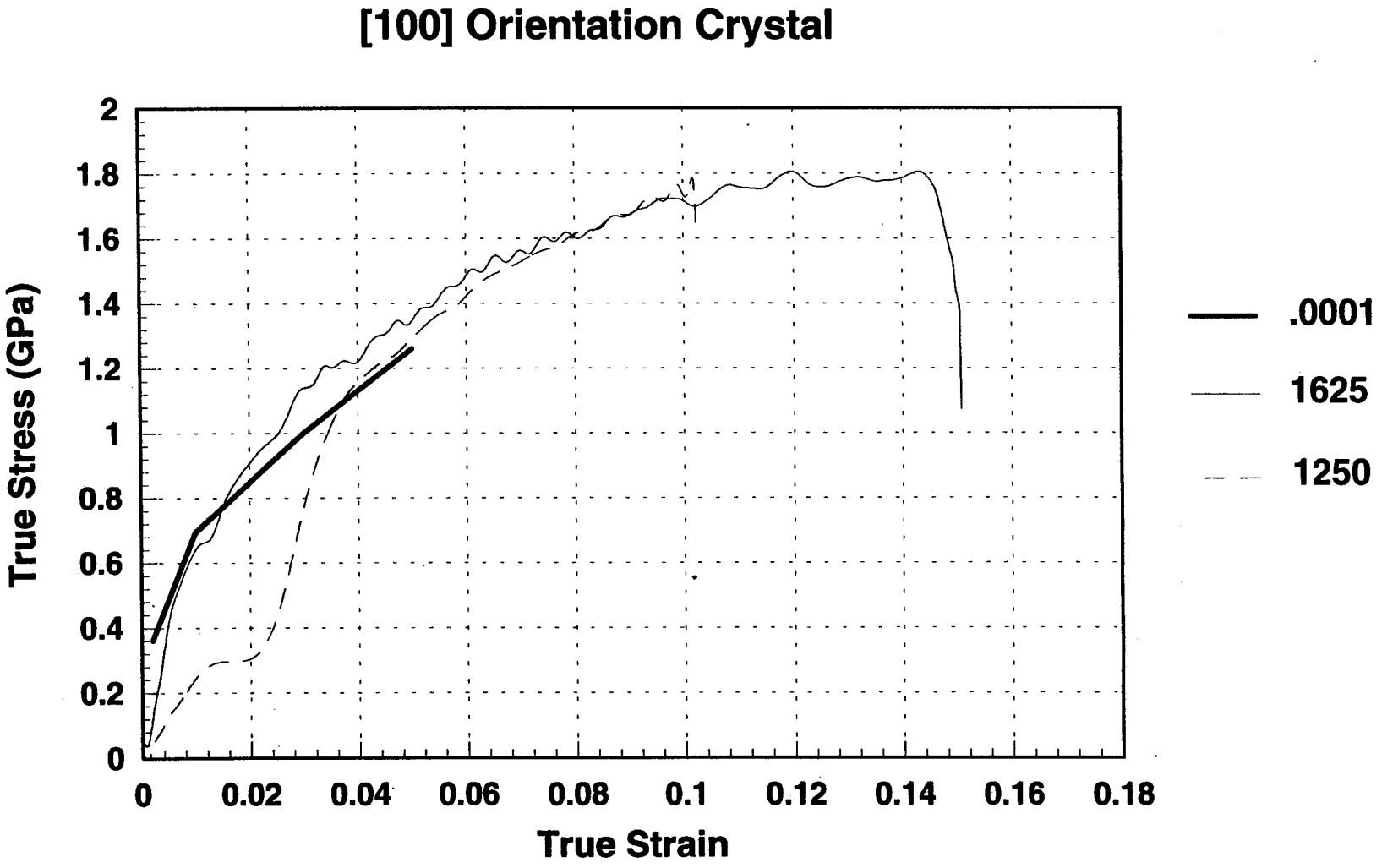

Figure 26. Comparison of true stress vs. true strain curves.

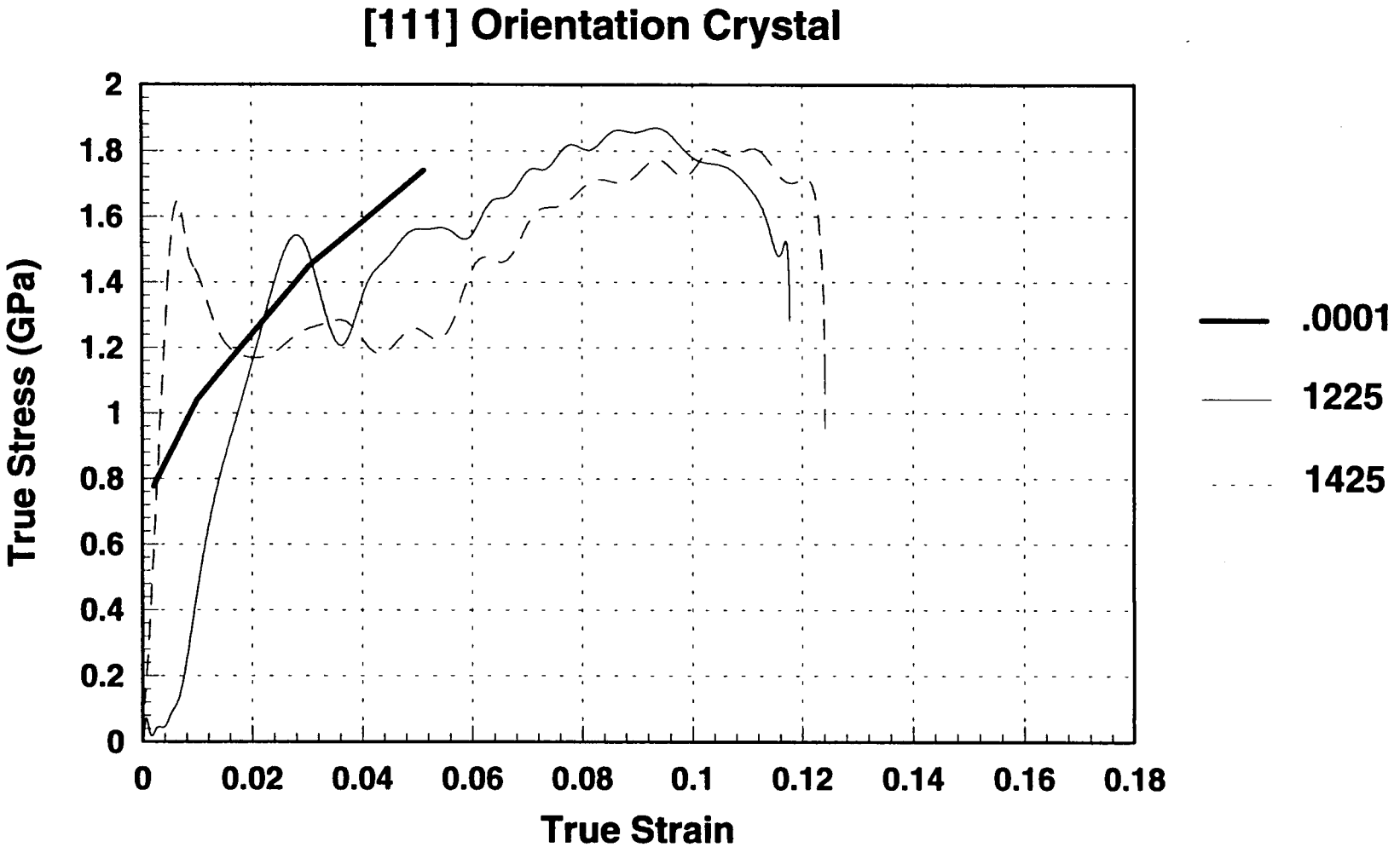

Figure 27. Comparison of true stress vs. true strain curves.

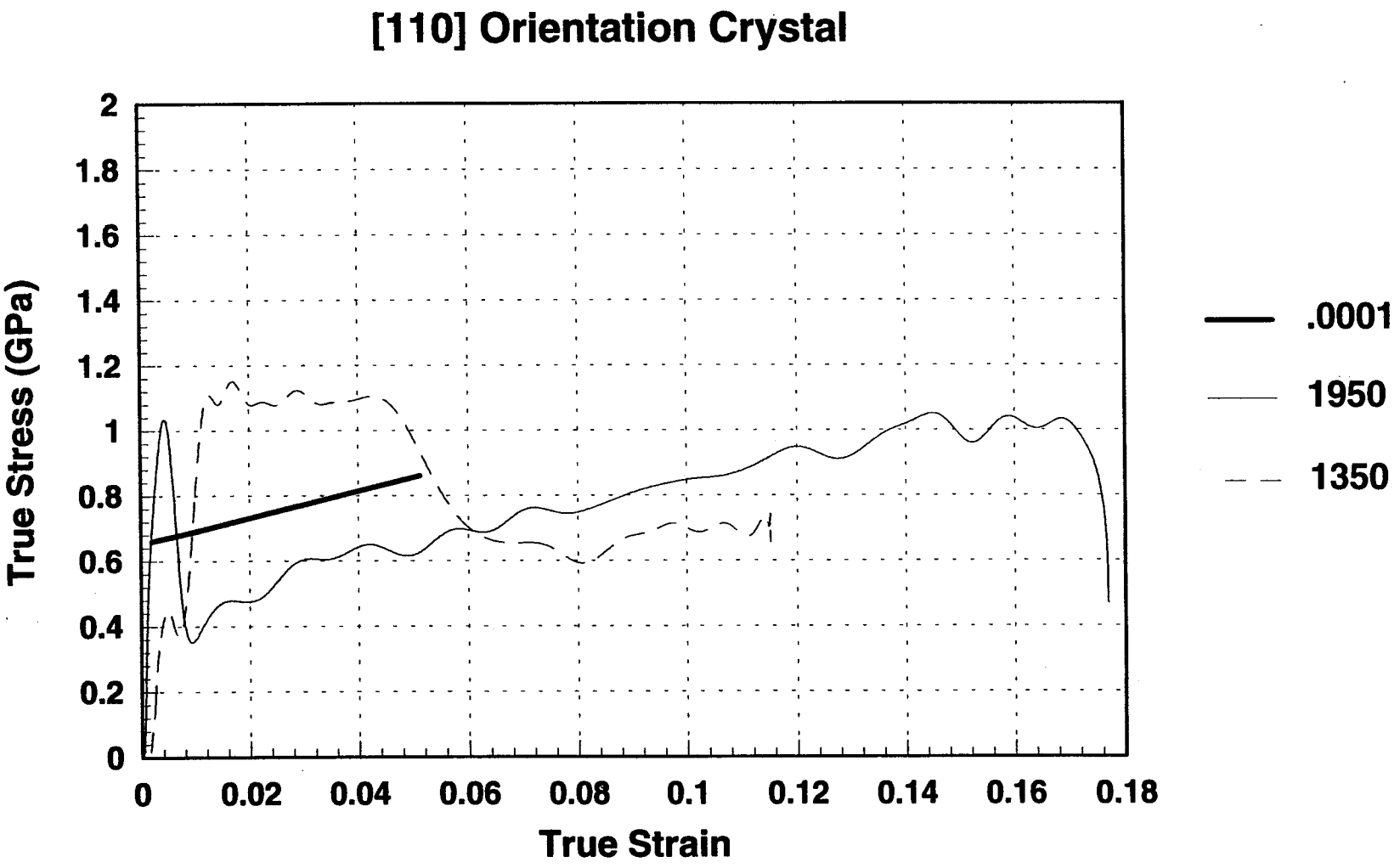

Figure 28. Comparison of true stress vs. true strain curves.

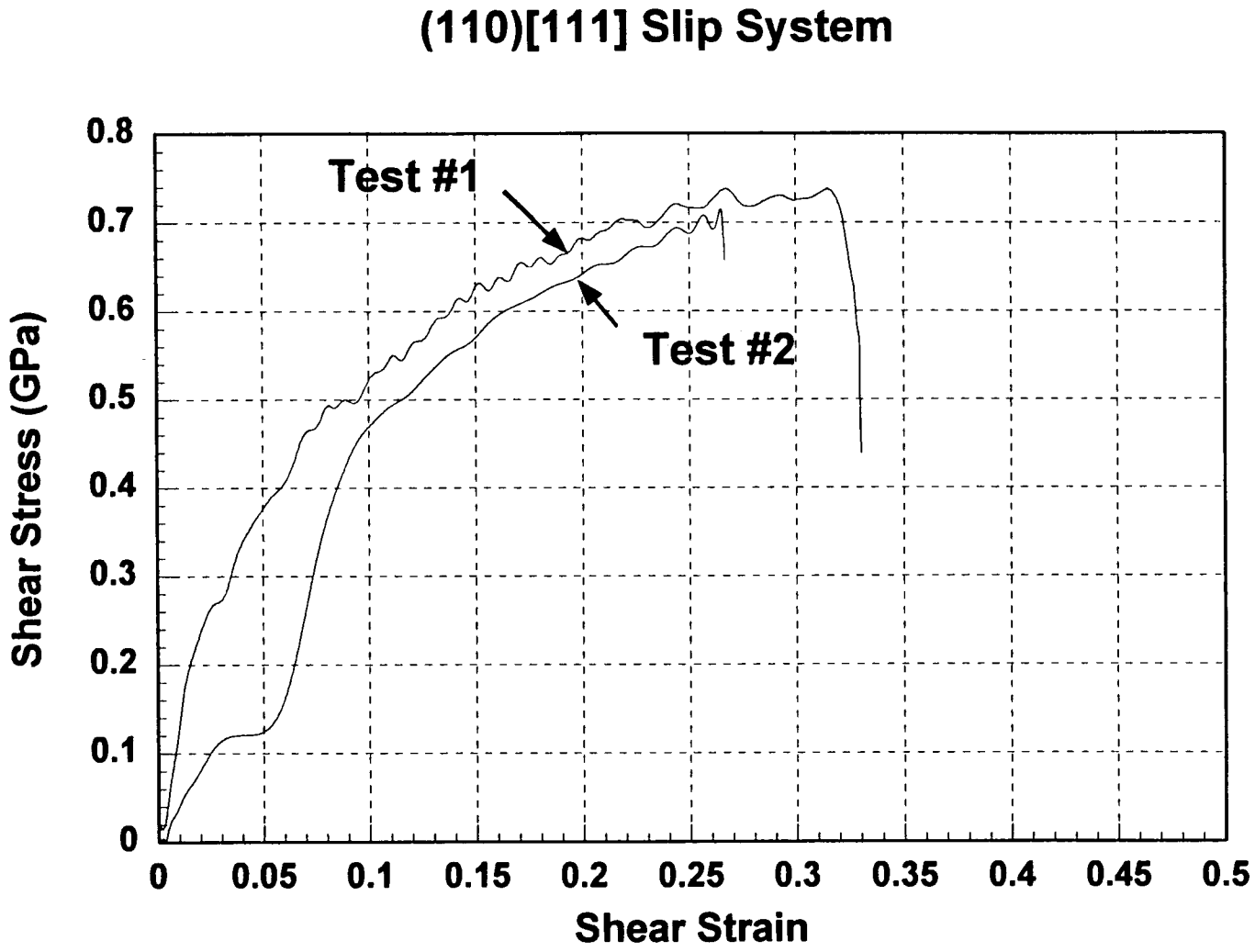

Figure 29. [100] crystals - shear stress vs. shear strain.

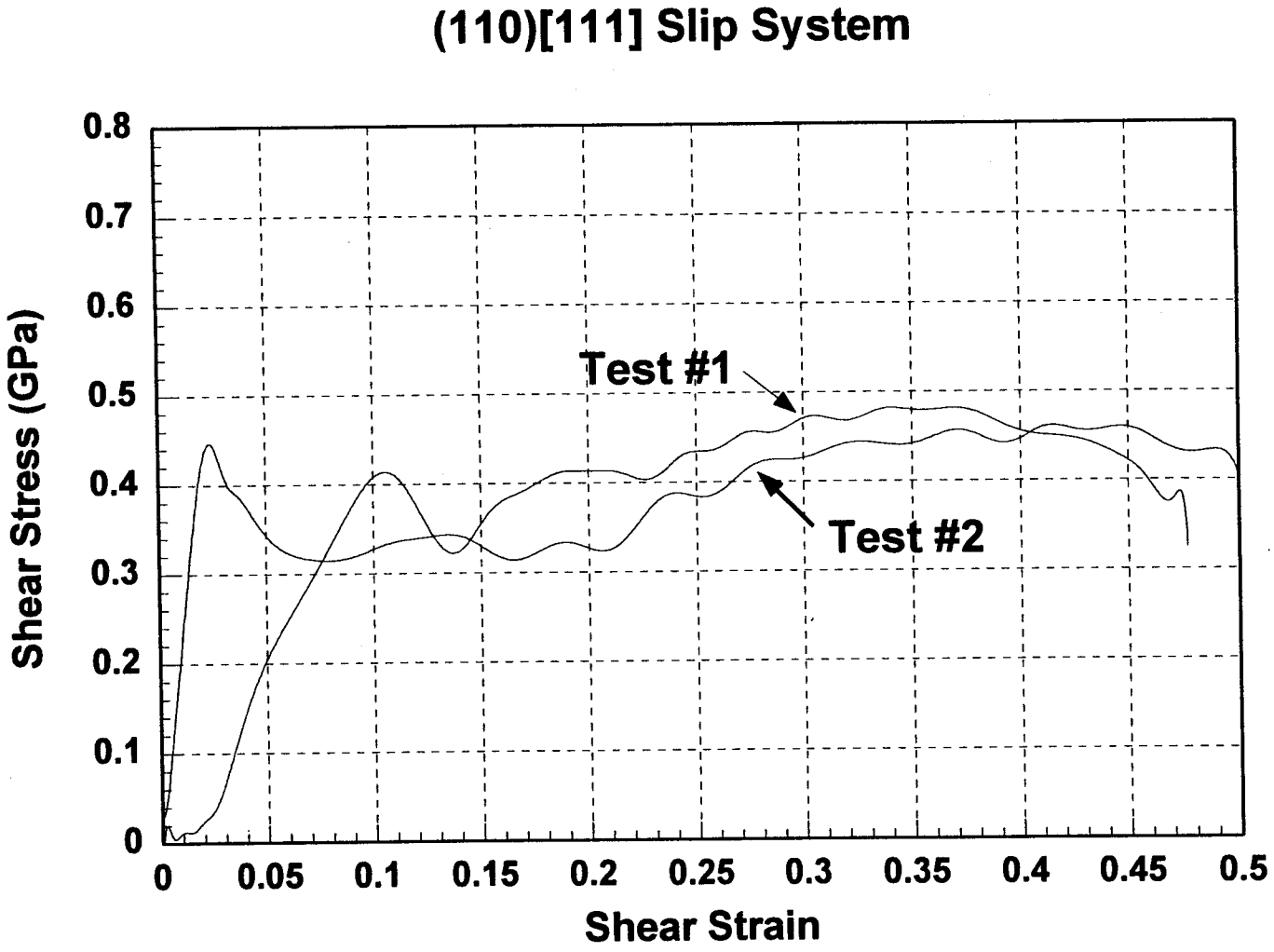

Figure 30. [111] crystals - shear stress vs. shear strain.

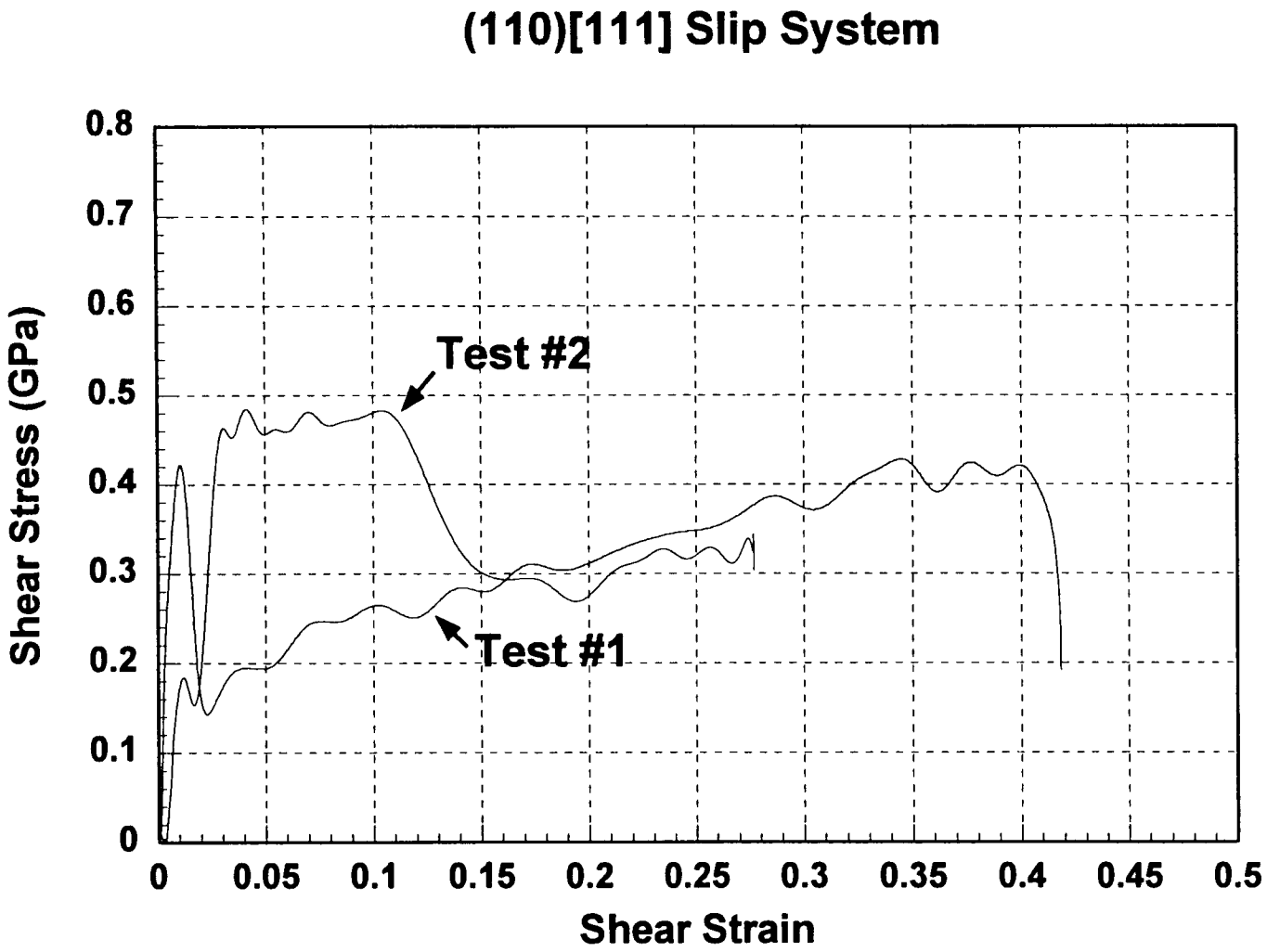

Figure 31. [110] crystals - shear stress vs. shear strain.

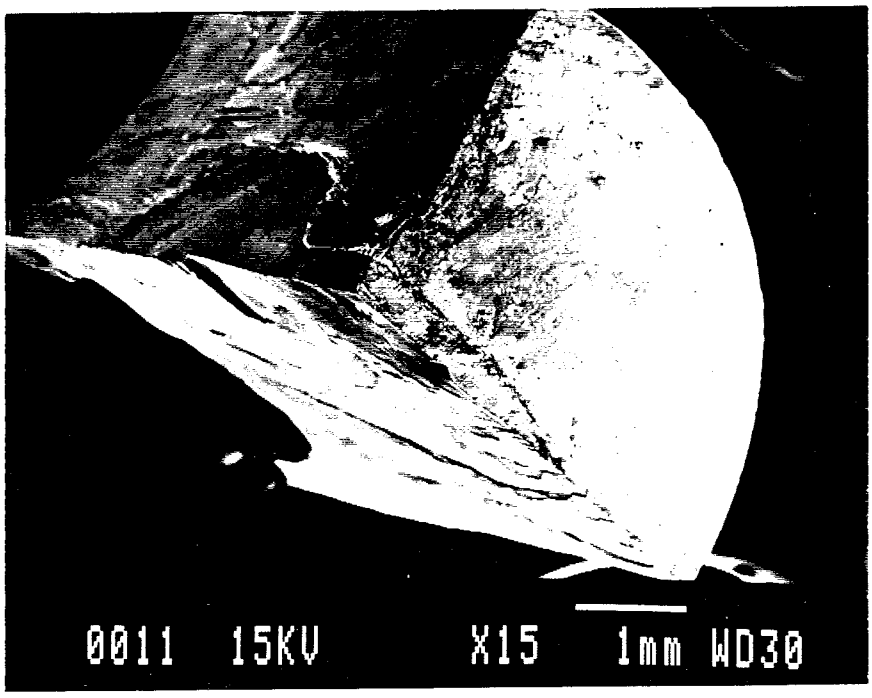

Figure 32a. [100] crystal - cleavage surface.

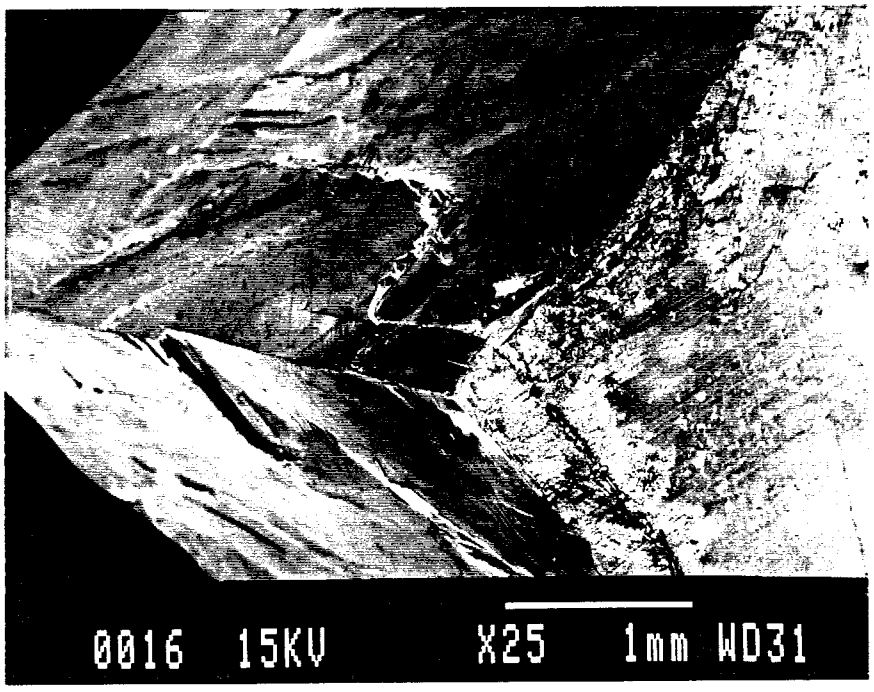

Figure 32b. [100] crystal - cleavage surface.

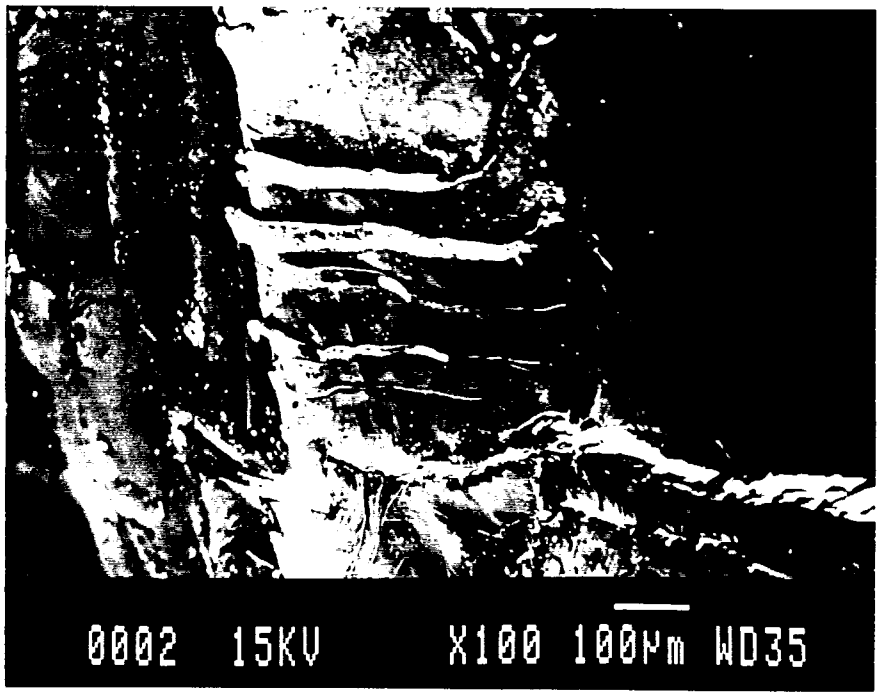

Figure 33. [100] crystal - slip on parallel planes.

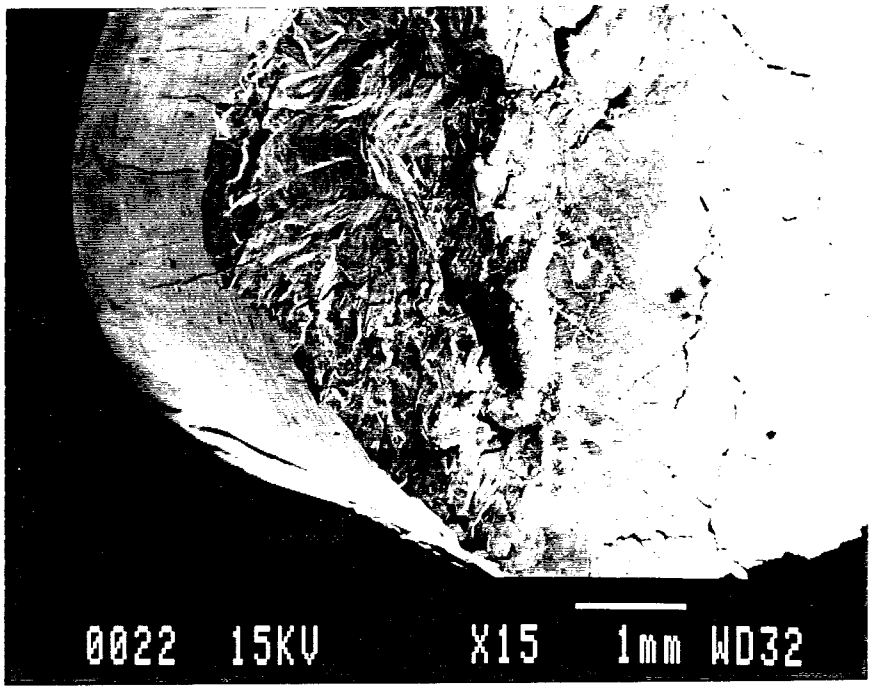

Figure 34a. [111] crystal - fracture surface.

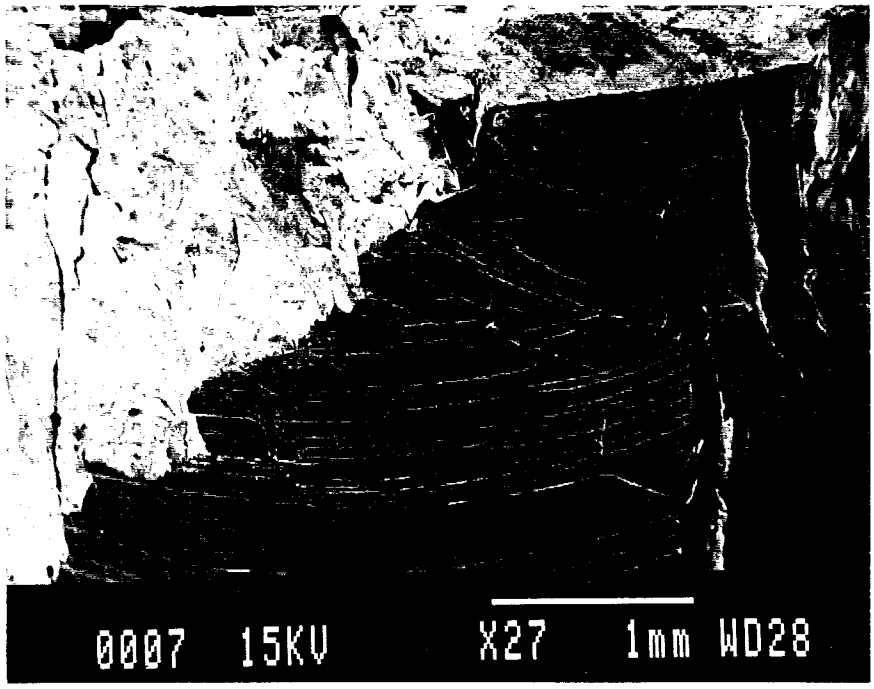

Figure 34b. [111] crystal - fracture surface and slip plane markings.

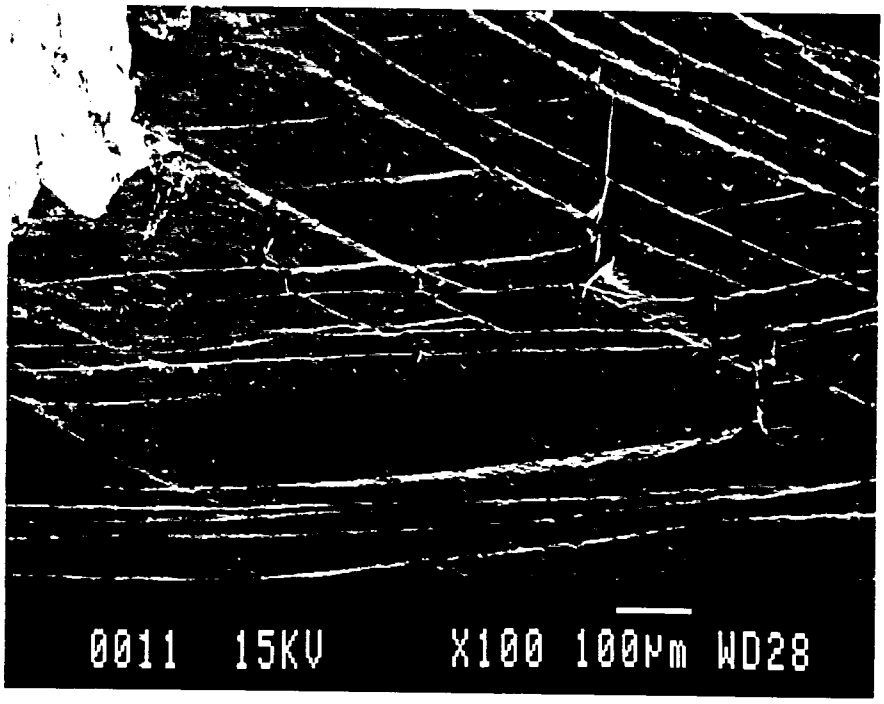

Figure 35a. [111] crystal - slip plane traces on surface.

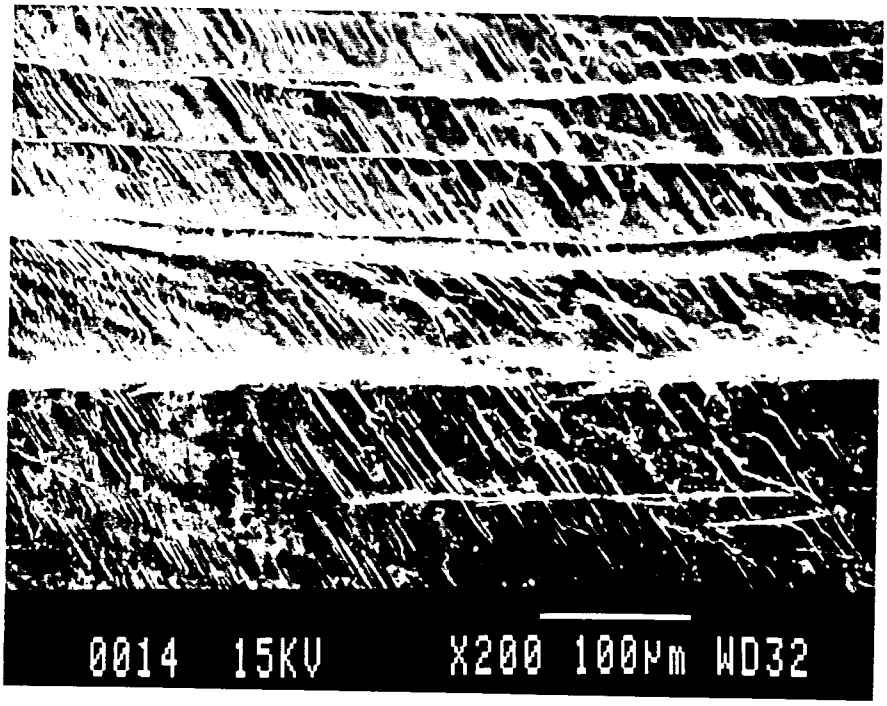

Figure 35b. [111] crystal - slip plane traces on surface.

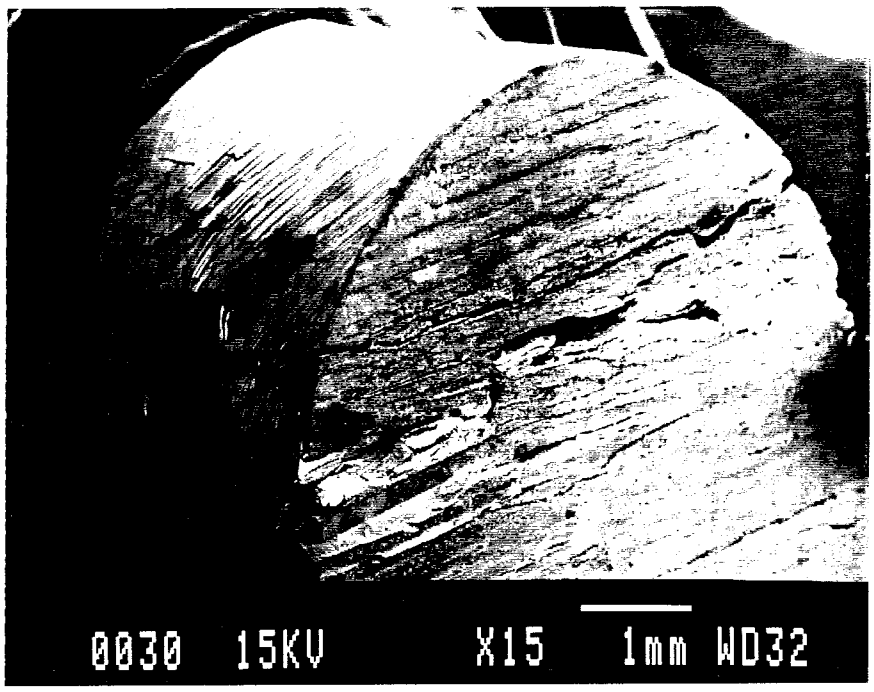

Figure 36a. [110] crystal - slip traces and cleavage.

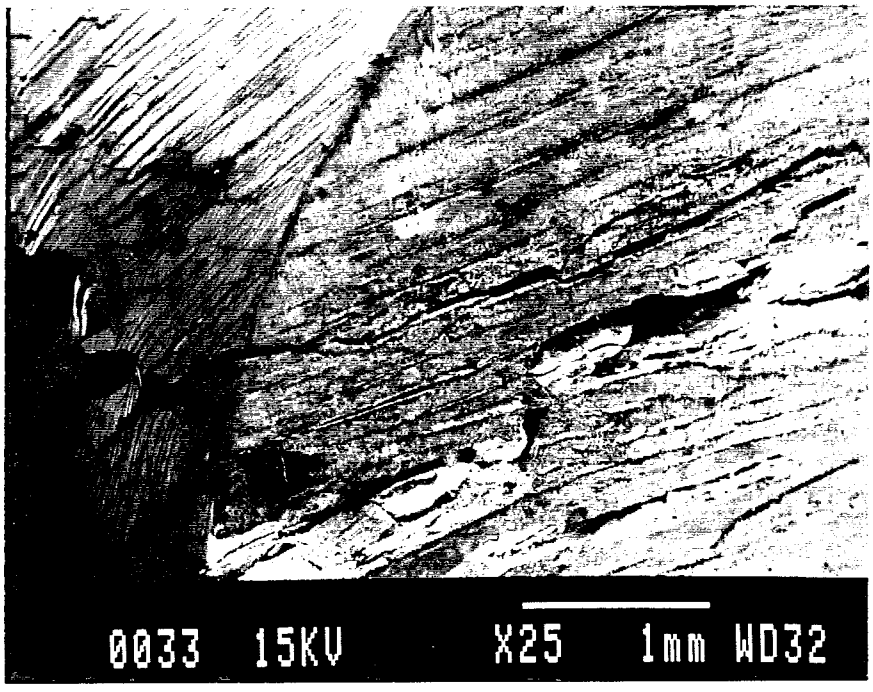

Figure 36b. [110] crystal - slip traces and cleavage.

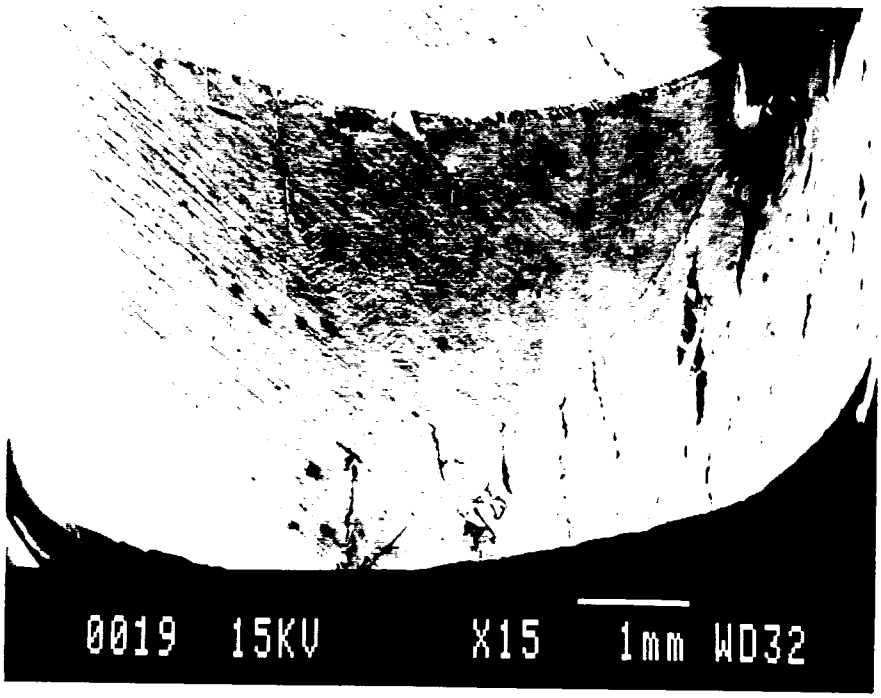

Figure 37a. [110] crystal - slip traces.

Figure 37b. [110] crystal - slip traces and failure voids.

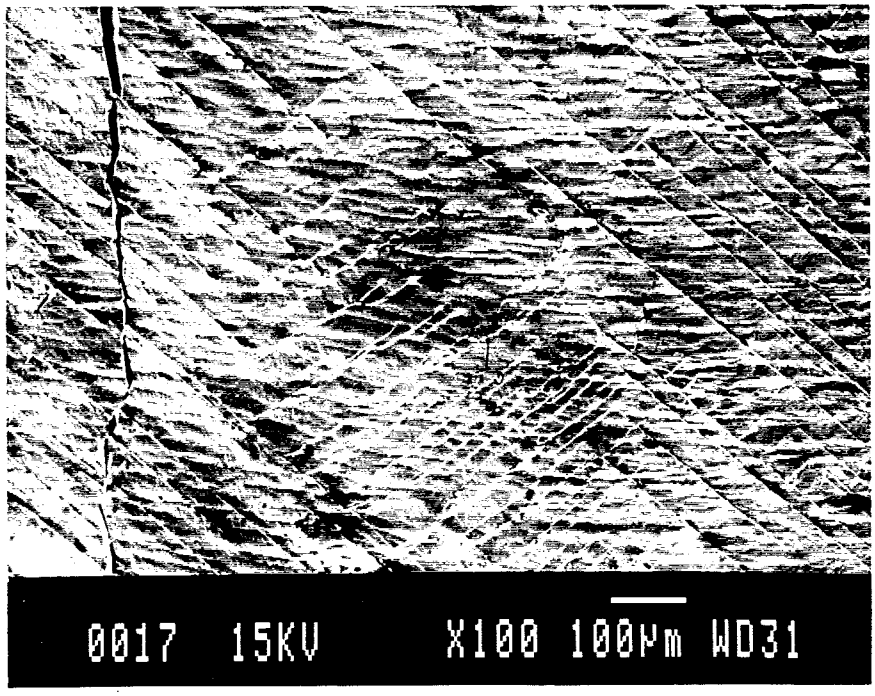

Figure 38a. [110] crystal - slip traces/specimen surface.

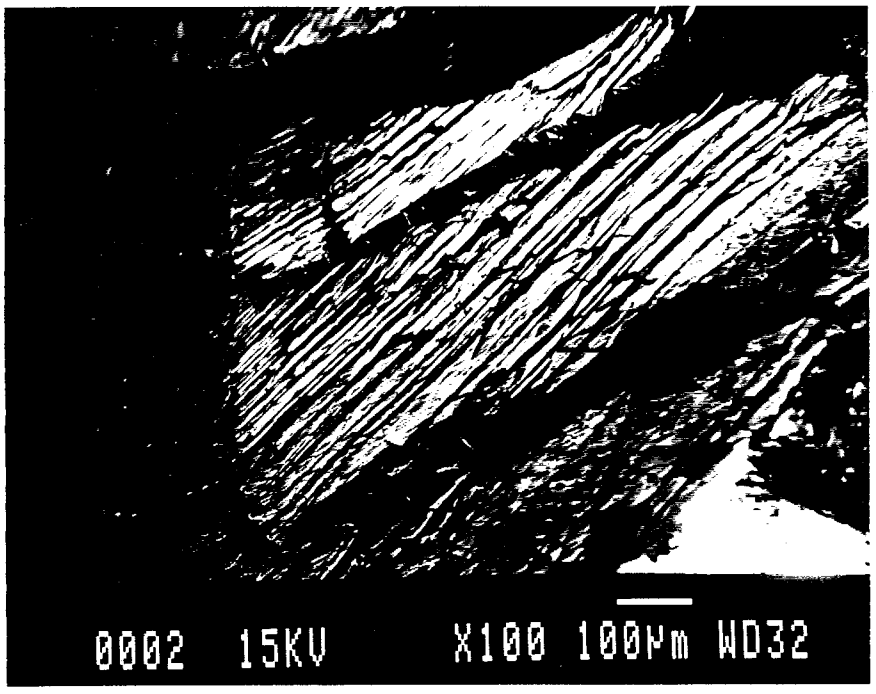

Figure 38b. [110] crystal - slip traces/specimen surface.

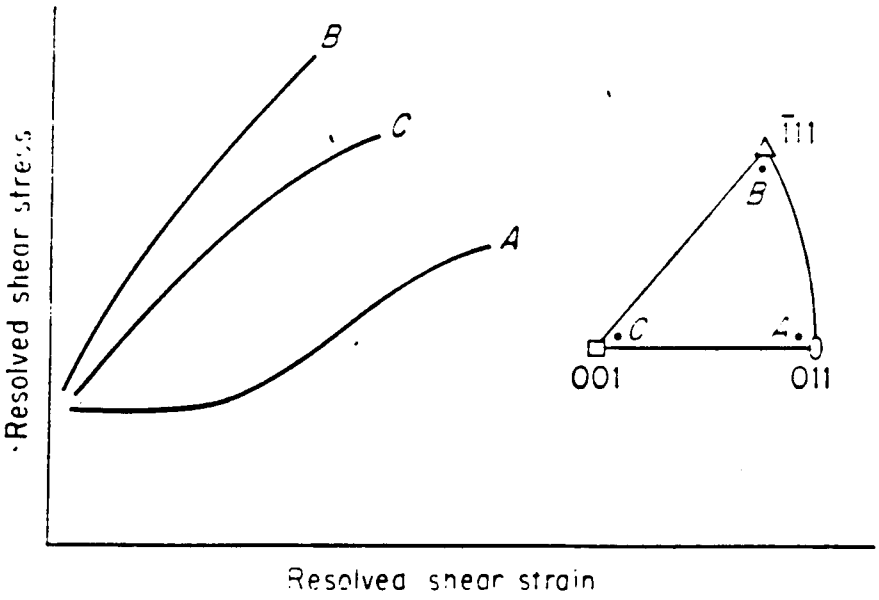

Figure 39. Effect of specimen orientation on the shape of the flow curve for fcc single crystals.

7. REFERENCES

Argon, A. S., and S. R Maloof. "Plastic Deformation of Tungsten Single Crystals at Low Temperatures." ACTA Metallurgica, vol. 14, p. 1449, 1966.

Beardmore, P., and D. Hull. "Deformation and Fracture of Tungsten Single Crystals." Journal of the Less-Common Metals," vol. 9, p. 168, 1965.

Bertholf and Karnes. "Two-Dimensional Analysis of the Split-Hopkinson Pressure Bar." Journal of the Mechanics and Physics of Solids, vol. 23, pp. 1–19, 1975.

Bowen, D. K., and J. W. Christian. "The Calculation of Shear Stress and Shear Strain for Double Glide in Tension and Compression." Philosophical Magazine, vol. 12, no. 116, p. 369, August 1965.

Bruchey, W. J., R. N. Herring, P. W. Kingman, and E. J. Horwath. "Deformation Mechanisms in Tungsten Single Crystals in Ballistic Impact Experiments." ARL-TR-133, U.S. Army Research Laboratory, Aberdeen Proving Ground, MD, May 1993.

Bruchey, W. J., E. J. Horwath, and W. R. Rowe. "The Effect of Crystallographic Orientation on the Performance of Single Crystal Tungsten Subscale Penetrators." ARL-MR-89, U.S. Army Research Laboratory, Aberdeen Proving Ground, MD, August 1993.

Coates, R. S., and K. T. Ramesh. "The Rate Dependent Deformation of a Tungsten Heavy Alloy." Materials Science and Engineering A, Vol. 145, 1991, pp. 159–166.

Cottrell, A. H. "Dislocations and Plastic Flow in Crystals." Oxford Press, 1953.

Davies, E. D., and S. C. Hunter. "The Dynamic Compression Testing of Solids by Method of the Split-Hopkinson Pressure Bar." Journal of the Mechanics and Physics of Solids, vol. 11, p. 155, 1963.

Dieter, G. E. Mechanical Metallurgy. New York: McGraw-Hill Book Company, 1986.

Follansbee, P. S., and C. Frantz. "Wave Propagation in the Split-Hopkinson Pressure Bar." Journal of Engineering Materials and Technology, vol. 105, p. 61, January 1983.

Garlick, R. G., and H. B. Probst. "Investigation of Room Temperature Slip on Zone Melted Tungsten Single Crystals." Trans AIME, vol. 230, p. 1120, 1964.

Herring, R. A. "Determination of Operable Deformation Mechanisms During Ballistic Impact in Tungsten Single Crystals Utilizing Transmission Electron Microscopy." BRL-TR-3385, U.S. Army Ballistic Research Laboratory, Aberdeen Proving Ground, MD, August 1992.

Kolsky, H. "An Investigation of the Mechanical Properties of Materials at Very High Rates of Loading." Proceedings of the Physical Society, vol. 62, p. 676, 1949.

Leslie, W. C. Metallurgical Effects at High Strain Rates. Edited by R. W. Rhode, B. M. Butcher, R. J. Holland, C. H. Karnes. New York: Plenum Press, 1973.

Li, G. The Johns Hopkins University, unpublished work, 1989.

Lindholm, U. S. "Some Experiments With the Split-Hopkinson Pressure Bar." Journal of the Mechanics and Physics of Solids, vol. 12, p. 317, 1964.

Rose, R. M., D. P. Ferriss, and J. Wulff. "Yielding and Plastic Flow in Single Crystals of Tungsten." Trans AIME, vol. 224, p. 981, 1962.

Weertman, J., and J. R. Weertman. "Elementary Dislocation Theory." MacMillan Series in Material Science, 1965.

NO. OF COPIES	ORGANIZATION
2	ADMINISTRATOR DEFENSE TECHNICAL INFO CENTER ATTN: DTIC-DDA CAMERON STATION ALEXANDRIA VA 22304-6145
1	COMMANDER US ARMY MATERIEL COMMAND ATTN: AMCAM 5001 EISENHOWER AVE ALEXANDRIA VA 22333-0001
1	DIRECTOR US ARMY RESEARCH LABORATORY ATTN: AMSRL-OP-SD-TA/ RECORDS MANAGEMENT 2800 POWDER MILL RD ADELPHI MD 20783-1145
3	DIRECTOR US ARMY RESEARCH LABORATORY ATTN: AMSRL-OP-SD-TL/ TECHNICAL LIBRARY 2800 POWDER MILL RD ADELPHI MD 20783-1145
1	DIRECTOR US ARMY RESEARCH LABORATORY ATTN: AMSRL-OP-SD-TP/ TECH PUBLISHING BRANCH 2800 POWDER MILL RD ADELPHI MD 20783-1145
2	COMMANDER US ARMY ARDEC ATTN: SMCAR-TDC PICATINNY ARSENAL NJ 07806-5000
1	DIRECTOR BENET LABORATORIES ATTN: SMCAR-CCB-TL WATERVLIET NY 12189-4050
1	DIRECTOR US ARMY ADVANCED SYSTEMS RESEARCH AND ANALYSIS OFFICE ATTN: AMSAT-R-NR/MS 219-1 AMES RESEARCH CENTER MOFFETT FIELD CA 94035-1000

NO. OF COPIES	ORGANIZATION
1	COMMANDER US ARMY MISSILE COMMAND ATTN: AMSMI-RD-CS-R (DOC) REDSTONE ARSENAL AL 35898-5010
1	COMMANDER US ARMY TANK-AUTOMOTIVE COMMAND ATTN: AMSTA-JSK (ARMOR ENG BR) WARREN MI 48397-5000
1	DIRECTOR US ARMY TRADOC ANALYSIS COMMAND ATTN: ATRC-WSR WSMR NM 88002-5502
1	COMMANDANT US ARMY INFANTRY SCHOOL ATTN: ATSH-WCB-O FORT BENNING GA 31905-5000
	ABERDEEN PROVING GROUND
2	DIR, USAMSAA ATTN: AMXSY-D AMXSY-MP/H COHEN
1	CDR, USATECOM ATTN: AMSTE-TC
1	DIR, USAERDEC ATTN: SCBRD-RT
1	CDR, USACBDCOM ATTN: AMSCB-CII
1	DIR, USARL ATTN: AMSRL-SL-I
5	DIR, USARL ATTN: AMSRL-OP-AP-L

NO. OF COPIES	ORGANIZATION
1	HQDA (SARD-TT/DR F MILTON) WASH DC 20310-0103
1	HQDA (SARD-TT/MR J APPEL) WASH DC 20310-0103
	ABERDEEN PROVING GROUND
14	DIR, USARL ATTN: AMSRL-WT-TA/ W BRUCHEY W GILLICH E HORWATH (10 CP) AMSRL-WT-TC/L MAGNESS AMSRL-WT-TD/A DIETRICH

USER EVALUATION SHEET/CHANGE OF ADDRESS

This Laboratory undertakes a continuing effort to improve the quality of the reports it publishes. Your comments/answers to the items/questions below will aid us in our efforts.

1. ARL Report Number ARL-TR-620 Date of Report November 1994

2. Date Report Received _____

3. Does this report satisfy a need? (Comment on purpose, related project, or other area of interest for which the report will be used.) _____

4. Specifically, how is the report being used? (Information source, design data, procedure, source of ideas, etc.) _____

5. Has the information in this report led to any quantitative savings as far as man-hours or dollars saved, operating costs avoided, or efficiencies achieved, etc? If so, please elaborate. _____

6. General Comments. What do you think should be changed to improve future reports? (Indicate changes to organization, technical content, format, etc.) _____

CURRENT ADDRESS

_____
Organization

_____
Name

_____
Street or P.O. Box No.

_____
City, State, Zip Code

7. If indicating a Change of Address or Address Correction, please provide the Current or Correct address above and the Old or Incorrect address below.

OLD ADDRESS

_____
Organization

_____
Name

_____
Street or P.O. Box No.

_____
City, State, Zip Code

(Remove this sheet, fold as indicated, tape closed, and mail.)
(DO NOT STAPLE)

DEPARTMENT OF THE ARMY

OFFICIAL BUSINESS

NO POSTAGE
NECESSARY
IF MAILED
IN THE
UNITED STATES

BUSINESS REPLY MAIL
FIRST CLASS PERMIT NO 0001, APG, MD

Postage will be paid by addressee

Director
U.S. Army Research Laboratory
ATTN: AMSRL-OP-AP-L
Aberdeen Proving Ground, MD 21005-5066